Manipulation of magnetic systems by quantized surface acoustic waves via the piezomagnetic effect

Yu-Yuan Chen,[1,2] Jia-Heng Wang,[1,2] Lu Ning Song,[1,2] and Yu-xi Liu[1,2,*]

[1] *School of Integrated Circuits, Tsinghua University, Beijing 100084, China*
[2] *Frontier Science Center for Quantum Information, Beijing 100084, China*

(Received 16 April 2024; accepted 28 January 2025; published 7 March 2025)

Quantized surface acoustic waves (SAWs) in piezoelectric media have been studied recently, and they can be used to control the electric dipoles of quantum systems via the electric field produced through the piezoelectric effect. However, it is not easy nor convenient to manipulate magnetic moments directly by an electric field. Here we study a quantum theory of SAWs in a piezomagnetic medium. We show that the intrinsic properties of the piezomagnetic medium enable the SAW in the piezomagnetic medium to interact directly with magnetic moments of quantum systems via the magnetic field induced by the piezomagnetic effect. By taking a strip SAW waveguide made of a piezomagnetic medium as an example, we further study the coupling strengths between different magnetic quantum systems with magnetic moments and the quantized single-mode SAW in the waveguide. Based on this, we discuss the interaction between magnetic quantum systems mediated by a quantized multimode SAW in a piezomagnetic waveguide. Our study provides a convenient way to directly control magnetic quantum systems by quantized SAWs, and offers potential applications to on-chip information processing based on solid-state quantum systems via quantized acoustic waves.

DOI: 10.1103/PhysRevApplied.23.034013

I. INTRODUCTION

A surface acoustic wave (SAW), a type of mechanical wave, propagates along the surface of an elastic medium with wave vectors orthogonal to the normal direction to the surface and is confined near the surface with a depth of about one wavelength [1–3]. Compared with electromagnetic waves, a SAW has about five orders of reduction in the propagation velocity (typically 3×10^3 m/s for a SAW instead of 3×10^8 m/s for an electromagnetic wave). That means the wavelength of a SAW is about five orders smaller than that of electromagnetic waves at the same frequency. These features mean that SAWs have a wide range of applications, e.g., modern electronic communication (such as radar, resonator, bandpass filter, and delay lines) [1–3], microfluid manipulation [4–6], cell manipulation [7–9], and sensors [10–12].

Quantum acoustics [13–19], which is an interdisciplinary research field of quantum mechanics and mechanical waves including SAWs, mainly studies the quantum effects of mechanical vibrations and the interaction between quantized mechanical vibrations and various quantum systems, including superconducting circuits [20–22], trapped ions [23–25], defect centers in diamond [26–28], and quantum dots [29–31]. A phonon is a quantum of vibrational mechanical energy in quantized mechanical vibrations. Note that superconducting circuits [32–36] have become one of the promising scalable solid-state platforms for realizing quantum computers. With the rapid development of fabrication technology for SAW devices and superconducting circuits, attention has been paid to achieve strong coupling between superconducting circuits and quantized single-mode SAWs at single-phonon level. Over the past few years, the quantized single-mode SAW has been studied experimentally and theoretically for quantum entanglement [19,37,38], quantum transduction [15,39,40], quantum routing [41–43], phononic blockade [44–46], and interaction with giant atoms [47–49].

So far, most existing research in SAW-based quantum acoustics has focused on the quantization of SAWs in a piezoelectric medium [13], as well as the coupling between quantum systems and a single-mode (or multimode) SAW in a resonator, which is formed by two reflecting gratings fabricated on the surface of a piezoelectric medium [13–22,25–31,37–49]. Thus, the coupling of a SAW to quantum systems is realized via the electric field produced through the piezoelectric effect. However, the magnetic moments of magnetic quantum systems (e.g., a superconducting qubit and a defect center in diamond) cannot be directly coupled to a SAW via the piezoelectric effect. To solve this problem, one possible solution is to deposit a magnetic film on the surface of the piezoelectric medium

*Contact author: yuxiliu@mail.tsinghua.edu.cn

[50–53]. Then, the SAW can be directly coupled to the spins in the magnetic film, and then indirectly coupled to magnetic quantum systems outside the magnetic film via the magnetic field produced by the magnetic film through the magnetoelastic effect. However, such a mediating magnetic film typically exhibits larger damping than the acoustic damping in the piezoelectric medium. Thus the SAW would suffer from larger damping when it is coupled to the magnetic film via the magnetoelastic effect. Note that when the mediating magnetic film on the piezoelectric medium is replaced by a well-designed film with multilayer magnetic materials, one can achieve strong coupling between the SAW (in the piezoelectric medium) and spins in the multilayer magnetic film [54–56]. This strong coupling may also result in indirect strong coupling between the SAW and other magnetic quantum systems outside the film.

In contrast to the SAW in a piezoelectric medium, the SAW in a piezomagnetic medium [57–59] offers a direct way to couple the SAW with magnetic quantum systems via the magnetic field induced by the piezomagnetic effect. The quantum theory of SAWs in piezoelectric media has been developed [13]. However, no detailed study on the quantum theory of SAWs in a piezomagnetic medium has been found. Thus, here we use a similar way as in Ref. [13] and employ the canonical quantization method [60,61] to study the quantum theory of SAWs in a piezomagnetic medium. The derivation is based on the classical SAW in a piezomagnetic medium, which is obtained by solving the general wave equations in a strip waveguide made of piezomagnetic medium. Based on this, we study the interaction between several magnetic quantum systems and a quantized single-mode SAW in a piezomagnetic strip waveguide. Furthermore, we study the interaction between two qubits mediated by a quantized multimode SAW in a piezomagnetic strip waveguide.

The paper is organized as follows. In Sec. II, for completeness of the paper, we first give a brief summary of the acoustic wave equations and boundary conditions in a general piezomagnetic medium, and derive the typical Rayleigh-type SAW in a piezomagnetic strip waveguide. In Sec. III, we resort to the canonical quantization method to derive the quantum theory of a SAW in a piezomagnetic strip waveguide and discuss the zero-point fluctuation of the quantized SAW. In Sec. IV, the interaction between several typical magnetic quantum systems and a quantized single-mode SAW in a strip waveguide is studied; and the coupling strengths of the magnetic quantum systems to a quantized single-mode SAW at single-phonon level are compared and summarized. As further applications, in Sec. V, we study the information transfer and entanglement between two superconducting qubits mediated by SAW phonons in a piezomagnetic waveguide. A discussion of our study is presented in Sec. VI. Finally, the conclusion is given in Sec. VII. For conciseness and completeness of the paper, detailed derivations are provided in the Supplemental Material [62].

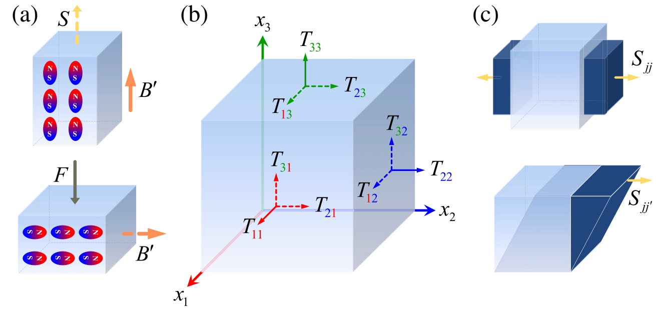

FIG. 1. (a) Schematic illustration for the (top) converse piezomagnetic effect and (bottom) piezomagnetic effect. (top) The external magnetic field B' results in the mechanical strain S and the alignment of magnetic moments inside the medium. (bottom) The mechanical strain S and the alignment of magnetic moments, produced by the externally applied force F, leads to the generation of magnetic field B'. The relation between the magnetic field B inside the medium and the magnetic field B' outside the medium is determined by the magnetic boundary condition in Eq. (5). (b) Schematic illustration for the normal stresses (solid arrows) and shear stresses (dashed arrows) acting on a unit cube. (c) Schematic illustration for the deformation of the (top) normal strains S_{jj} and (bottom) shear strains $S_{jj'}$ ($j' \neq j$) of a unit cube.

II. CLASSICAL SAW IN A PIEZOMAGNETIC MEDIUM

Within a piezoelectric medium, mechanical displacements or strains would induce electric fields via the piezoelectric effect. In a similar manner, within a piezomagnetic medium, mechanical displacements or strains would lead to the generation of magnetic fields via the piezomagnetic effect, as schematically shown in Fig. 1(a). In this section, for the completeness of the studies, we summarize several main results for classical SAWs in a strip waveguide made of a piezomagnetic medium.

A. Acoustic wave equations in a piezomagnetic medium and boundary conditions

In the following, we limit our discussion to the case of linear piezomagnetic coupling, which determines the basic properties of SAWs. In a general piezomagnetic medium, the propagation of acoustic waves is described by the coupled constitutive equations that connect the mechanical vibration and magnetic field as follows [57,58]

$$\begin{aligned} T_{ij} &= C_{ijkl}S_{kl} - q_{kij}H_k, \\ B_i &= \mu_{ik}H_k + q_{ijk}S_{jk}. \end{aligned} \tag{1}$$

Here, the first subscript of the stress tensor T_{ij} denotes the direction of the force exerted on the area under consideration, and the second one denotes the outward-going normal direction of the area on which the force is exerted, as schematically shown in Fig. 1(b). Each subscript can be 1, 2, or 3, which denote the x, y, or z direction, respectively; B_i is the magnetic induction along the x_i direction; C_{ijkl}, q_{kij}, and μ_{ik} represent the elastic stiffness, piezomagnetic, and magnetic permeability tensors, respectively; and $S_{jk} = (\partial u_j/\partial x_k + \partial u_k/\partial x_j)/2$ is the component of the strain S determined by the mechanical displacements u_j and u_k that are, respectively, along the x_j and x_k directions, as schematically shown in Fig. 1(c). Finally, H_k denotes the magnetic field strength H along the x_k direction. Here, the magnetic field $H_k = -\partial\psi/\partial x_k$ is determined only by the magnetic potential ψ under the quasistatic approximation [59,63], wherein the piezomagnetic coupling between acoustic and electromagnetic waves is negligible in comparison with the effect of piezomagnetic stiffening.

The equation of motion of particle displacement in a solid without body force is given by [1,3,58]

$$\rho\frac{\partial^2 u_i}{\partial t^2} = \frac{\partial T_{ij}}{\partial x_j}, \tag{2}$$

where ρ denotes the mass density of the medium. The magnetic induction B is described by the Maxwell equation, as follows [64]:

$$\nabla\cdot B = 0. \tag{3}$$

Here, we consider that the surface $z=0$ of the piezomagnetic medium is stress-free. That means the three components of stress exerted on the surface $z=0$ vanish, i.e.,

$$T_{13} = T_{23} = T_{33} = 0. \tag{4}$$

The magnetic induction B must be continuous across the surface of the medium [64], i.e.,

$$B_3(z\to 0^+) = B_3(z\to 0^-). \tag{5}$$

B. Rayleigh-type SAW in a cubic piezomagnetic strip waveguide

The Rayleigh-type SAW, which stands as a typical SAW [3,13,66,67], contains a longitudinal vibration and a transverse vibration, with a phase difference of $\pi/2$ between them. Hereafter, by taking a strip waveguide made of a piezomagnetic medium as an example, we consider the traveling-wave Rayleigh-type SAW propagating along the [110] direction of a cubic piezomagnetic material for convenience. Thus, the ansatzes of the mechanical displacements are given as (see Sec. I of the Supplemental Material [62])

$$\begin{aligned} u_{x'} &= \sum_k u_{x',k} = \sum_k U'_k e^{-kqz} e^{i(kx'-\omega_k t)}, \\ u_z &= \sum_k u_{z,k} = \sum_k iW_k e^{-kqz} e^{i(kx'-\omega_k t)}. \end{aligned} \tag{6}$$

Here, $k = 2\pi/\lambda_k$ denotes the wave number of the SAW with wavelength λ_k; $\sum_k$ denotes the summation over all allowed values of k range from negative infinity to positive infinity; $u_{x',k}$ and $u_{z,k}$ denote the components of the mechanical displacement, with amplitudes U'_k and W_k; q is a dimensionless complex parameter related to the decay of the SAW into the bulk; and $\omega_k = kv$ denotes the frequency of the SAW, with propagation velocity v. It should be noted that $u_{x',k}/\sqrt{2} = u_{1,k} = u_{2,k}$ is the displacement component along the redefined direction $x' = (x_1+x_2)/\sqrt{2}$, perpendicular to another redefined direction $y' = (x_2 - x_1)/\sqrt{2}$. Here, x' corresponds to the [110] direction of the crystal.

Specifically, we further take a cubic sample of terfenol-D [65], which can be considered as a piezomagnetic material under a weak driving field [65,68–72], as an example to further discuss the mechanical displacement and magnetic potential. By including the normalization condition for the ansatz in Eqs. (6) and the detailed structure of the piezomagnetic medium, we obtain the solutions of mechanical displacements in the waveguide as follows (see Sec. II of the Supplemental Material [62])

$$\begin{aligned} u_{x',k} &= 2U_{0,k}\cos(kq_\beta z + \theta)e^{-kq_\alpha z}e^{i(kx'-\omega_k t)}, \\ u_{z,k} &= -2iU_{0,k}|\gamma|\cos(q_\beta kz + \theta + \xi)e^{-kq_\alpha z}e^{i(kx'-\omega_k t)}, \end{aligned} \tag{7}$$

where the normalization constant $U_{0,k}$ will be further discussed in Sec. III D. The parameters q_α and q_β are, respectively, the real and imaginary parts of the dimensionless complex parameter q. Here, q_α characterizes the decay of the SAW into the bulk. The parameters $|\gamma|$ and ξ are determined by, respectively, the amplitude and argument of the complex ratio between the transverse and longitudinal mechanical displacements. The parameter θ is determined by the dimensionless complex parameter q and the complex ratio between the transverse and longitudinal displacements. Detailed expressions of the parameters $|\gamma|$, ξ, and θ can be found in Sec. II of the Supplemental Material [62].

In terms of the mechanical displacements in Eqs. (7), by solving the coupled equation in Eq. (3) and considering the magnetic boundary condition in Eq. (5), we obtain the solution for the magnetic potential in the waveguide given as (see Sec. II of the Supplemental Material [62])

$$\psi = \begin{cases} \sum_k i\psi_{0,k}F_k(z)e^{i(kx'-\omega_k t)}, & z \ge 0, \\ \sum_k i\psi_{0,k}F_k(z=0)e^{kz}e^{i(kx'-\omega_k t)}, & z < 0. \end{cases} \tag{8}$$

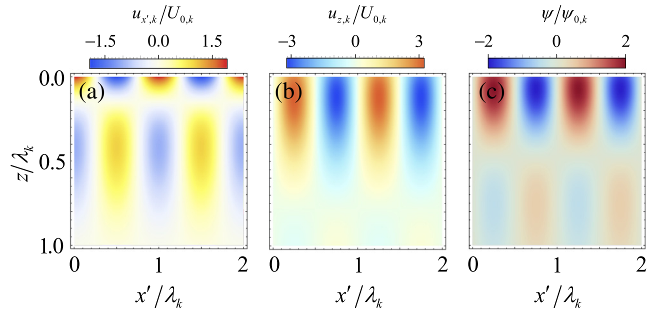

FIG. 2. The spatial distribution of (a) the longitudinal mechanical displacement $u_{x',k}$, (b) the transverse mechanical displacement $u_{z,k}$, and (c) the magnetic potential ψ_k for a SAW with wavelength λ_k. The other parameters are $\rho = 9.06$ g/cm^3, $C_{11} = 55$ GPa, $C_{12} = 43$ GPa, $C_{44} = 12$ GPa, $q_{31} = -45$ N/A m, $q_{33} = 90$ N/A m, and $\mu_{11} = 6.283$ μN/A^2.

Here, $\psi_{0,k} = q_{33}U_{0,k}/\mu_{11}$ is the amplitude of the magnetic potential; $F_k(z) = 2Ae^{-kq_\alpha z}\cos(kq_\beta z + \theta + \tau) + A_3e^{-kz}$ describes the depth scale on which the magnetic potential of SAW decays into the bulk; and A and A_3 are parameters related to the amplitude of the magnetic potential, while τ is a parameter related to the argument of the magnetic potential. Detailed expressions for the parameters A, A_3, and τ can be found in Sec. II of the Supplemental Material [62].

According to the parameters for terfenol-D given in Table I, the parameters in the solutions of the mechanical displacements in Eqs. (7) and the magnetic potential in Eqs. (8) are calculated as $v = 1005$ m/s, $q_\alpha = 0.4288$, $q_\beta = 0.5378$, $\theta = 1.0700$, $|\gamma| = 1.4116$, $\xi = -2.1401$, $A = 0.8437$, $\tau = 1.9172$, and $A_3 = 1.0370$. In order to study the properties of the Rayleigh-type SAW in a piezomagnetic medium, the dependence of the mechanical displacements and magnetic potential on the spatial positions x' and z is shown in Fig. 2. It is found that both the mechanical displacements and magnetic potential decay rapidly along the $+z$ direction, and their corresponding amplitudes approach zero near a depth of one wavelength. That is, the energy of the SAW is confined to near the surface of the medium. For the mechanical displacement of the SAW, there exists a phase difference $\pi/2$ between the longitudinal and transverse components, as shown in Figs. 2(a) and 2(b). Thus, for any particle within and near the surface of the medium, as the SAW propagates, it undergoes elliptical motion in the vicinity of its equilibrium position.

TABLE I. Density, elastic, piezomagnetic, and magnetic permeability properties for the material terfenol-D [65].

ρ (g/cm^3)	C_{11} (GPa)	C_{12} (GPa)	C_{44} (GPa)	q_{31} (N/A m)	q_{33} (N/A m)	μ_{11} (μN/A^2)
9.06	55	43	12	−45	90	6.283

Also, there is a phase difference $\pi/2$ between the longitudinal mechanical displacement and the magnetic potential, as shown in Figs. 2(a) and 2(c). Note that the properties exhibited here are similar to those of a Rayleigh-type SAW in a piezoelectric medium [1–3,13].

III. QUANTIZATION OF A SAW IN A PIEZOMAGNETIC WAVEGUIDE

We have obtained the solutions for the mechanical displacement and magnetic potential for a classical Rayleigh-type SAW in a piezomagnetic waveguide. Let us now apply the canonical quantization method [60,61] to achieve the quantization of a SAW in a piezomagnetic waveguide. To show the quantization process clearly, here we take a Rayleigh-type SAW in a cubic piezomagnetic material, terfenol-D, which was mentioned in Sec. II B, as an example to derive more detailed expressions. Here, it is worth pointing out that the employed canonical quantization method [60,61] is also applicable to the quantization of arbitrary types of SAWs in piezomagnetic materials.

A. Lagrangian of a SAW

The Lagrangian of a SAW propagating in a piezomagnetic medium is written as

$$\mathcal{L} = E_\mathrm{K} - E_\mathrm{P}, \tag{9}$$

where E_K and E_P denote, respectively, the kinetic energy and potential energy terms given as

$$E_\mathrm{K} = \int \frac{1}{2}\rho\frac{\partial u}{\partial t}\frac{\partial u^*}{\partial t}\,dV, \tag{10}$$

$$E_\mathrm{P} = \int \frac{1}{2}(S\cdot T - H\cdot B)\,dV. \tag{11}$$

In terms of the generalized coordinates $u_{x'}$, u_z, and ψ, the detailed expressions of the kinetic energy and potential energy terms are given as follows:

$$\begin{aligned}
E_\mathrm{K} &= \int \frac{1}{2}\rho\left[\frac{\partial u_{x'}}{\partial t}\frac{\partial u_{x'}^*}{\partial t} + \frac{\partial u_z}{\partial t}\frac{\partial u_z^*}{\partial t}\right]dV,\\
E_\mathrm{P} &= \int \frac{1}{2}\left[C'_{11}\left(\frac{\sqrt{2}\,\partial u_{x'}}{\partial x_1}\right)^2 + C_{44}\left(\frac{\partial u_{x'}}{\partial x_3} + \frac{\sqrt{2}\,\partial u_z}{\partial x_1}\right)^2\right]dV\\
&\quad + \int \frac{1}{2}\left[C_{11}\left(\frac{\partial u_z}{\partial x_3}\right)^2 + 2C_{12}\frac{\sqrt{2}\,\partial u_{x'}}{\partial x_1}\frac{\partial u_z}{\partial x_3}\right]dV\\
&\quad - \int \frac{1}{2}\left[\mu_{11}\left(\frac{\sqrt{2}\,\partial\psi}{\partial x_1}\right)^2 + \mu_{11}\left(\frac{\partial\psi}{\partial x_3}\right)^2\right]dV\\
&\quad - \int\left(q_{31}\frac{\sqrt{2}\,\partial u_{x'}}{\partial x_1}\frac{\partial\psi}{\partial x_3} + q_{33}\frac{\partial u_z}{\partial x_3}\frac{\partial\psi}{\partial x_3}\right)dV.
\end{aligned} \tag{12}$$

B. Canonical coordinates and canonical momenta of the SAW

For the Rayleigh-type SAW, there exists a phase difference $\pi/2$ between $u_{x'}$ and u_z, as well as between $u_{x'}$ and ψ. If $u_{x'}$, u_z, and ψ are chosen as the canonical coordinates, such a phase difference would lead to noncommutation between different coordinates. Therefore, $u_{x'}$, u_z, and ψ are a set of generalized coordinates rather than canonical coordinates.

In our study, quantization of the SAW is achieved via the canonical quantization method [60,61], which uses canonical coordinates and canonical momenta. For a given system, the canonical coordinates and corresponding canonical momenta are not unique, but they are required to satisfy the equations of motion and the fundamental Poisson bracket relations. Therefore, we consider transforming the generalized coordinates $u_{x'}$, u_z, and ψ to new coordinates, such that the new coordinates commute with each other in the Lagrangian.

The spatial derivatives of the mechanical displacements and magnetic potential are given in terms of themselves as (see Sec. III of the Supplemental Material [62])

$$\begin{aligned}
\frac{\partial u_{x'}(\boldsymbol{r})}{\partial x_1} &= \sum_{k>0} k g_k^{(1)} u_{z,k}(\boldsymbol{r}), & \frac{\partial u_{x'}(\boldsymbol{r})}{\partial x_3} &= \sum_{k>0} k g_k^{(2)} u_{x',k}(\boldsymbol{r}),\\
\frac{\partial u_{z}(\boldsymbol{r})}{\partial x_1} &= \sum_{k>0} k g_k^{(3)} u_{x',k}(\boldsymbol{r}), & \frac{\partial u_{z}(\boldsymbol{r})}{\partial x_3} &= \sum_{k>0} k g_k^{(4)} u_{z,k}(\boldsymbol{r}),\\
\frac{\partial \psi(\boldsymbol{r})}{\partial x_1} &= \sum_{k>0} k g_k^{(5)} u_{x',k}(\boldsymbol{r}), & \frac{\partial \psi(\boldsymbol{r})}{\partial x_3} &= \sum_{k>0} k g_k^{(6)} \psi_k(\boldsymbol{r}),
\end{aligned} \tag{13}$$

where the term $(\boldsymbol{r})$ denotes the spatial term of the generalized coordinates. The summation $\sum_{k>0}$ is over allowed values of the k range from zero to positive infinity. To find the canonical coordinates transformed from the generalized coordinates $u_{x'}$, u_z, and ψ, we substitute Eqs. (13) into Eqs. (12). Thus, the kinetic energy and potential energy terms can be rewritten as

$$\begin{aligned}
E_\mathrm{K} &= \int \sum_{k>0} \frac{1}{2}\rho \left(\frac{\partial u_{x',k}}{\partial t}, \frac{\partial u_{z,k}}{\partial t}\right)\left(\frac{\partial u^*_{x',k}}{\partial t}, \frac{\partial u^*_{z,k}}{\partial t}\right)^T dV,\\
E_\mathrm{P} &= \int \sum_{k>0} \frac{1}{2} k^2 (u_{x',k}, u_{z,k}, \psi_k) G_k(z) (u_{x',k}, u_{z,k}, \psi_k)^T dV,
\end{aligned} \tag{14}$$

where $G_k(z)$, given in Sec. III of the Supplemental Material [62], is the quadratic-form coefficient matrix constructed according to Eqs. (13).

To eliminate the cross terms of coordinates in the potential energy term in Eqs. (14), we take the orthogonal matrix $Q_k^{(1)}$ to diagonalize $G_k(z)$ such that

$$\begin{aligned}
\lambda_k^{(1)} &\equiv \mathrm{diag}(\lambda_{1,k}^{(1)}, \lambda_{2,k}^{(1)}, \lambda_{3,k}^{(1)})\\
&= Q_k^{(1)T} G_k(z) Q_k^{(1)},
\end{aligned} \tag{15}$$

where $Q_k^{(1)}$ is constructed via the eigenvector of the quadratic-form coefficient matrix $G_k(z)$. The eigenvalue $\lambda_{j,k}^{(1)}$ is the root of the secular equation $\det(G_k(z) - \lambda\mathbf{I}) = 0$, with the identity matrix $\mathbf{I}$. Therefore, the potential energy term in Eqs. (14) is written as

$$E_\mathrm{P} = \int \sum_{k>0} \frac{1}{2} k^2 X_k^{(1)T} Q_k^{(1)T} G_k(z) Q_k^{(1)} X_k^{(1)}\, dV, \tag{16}$$

where $X_k^{(1)} = [Q_k^{(1)}]^{-1}(u_{x',k}, u_{z,k}, \psi_k)^T$ denotes the coordinates transformed from the generalized coordinates $u_{x',k}$, $u_{z,k}$, and ψ_k via the orthogonal matrix $Q_k^{(1)}$. However, we note that $X_k^{(1)}$ is not the expected canonical coordinate since the transform $Q_k^{(1)}$ would lead to cross terms of coordinates in the kinetic energy term. That is,

$$E_\mathrm{K} = \int \sum_{k>0} \frac{1}{2}\rho \left[\frac{\partial X_k^{(1)}}{\partial t}\right]^T Y_k(z) \left[\frac{\partial X_k^{(1)}}{\partial t}\right] dV, \tag{17}$$

where $Y_k(z)$, given in Sec. III of the Supplemental Material [62], is constructed from the matrix $Q_k^{(1)}$ but is not a diagonal matrix.

Hence, it is necessary to further consider the coordinate transform via the orthogonal matrix $Q_k^{(2)}$, which ensures that no cross terms of transformed coordinates exist in both the kinetic energy and potential energy terms. Thus, we can construct the orthogonal matrix $Q_k^{(2)}$ via the normalized eigenvector of $[\lambda_k^{(1)}]^{-1} Y_k$, that is,

$$\begin{aligned}
\lambda_k^{(2)} &\equiv \mathrm{diag}(\lambda_{1,k}^{(2)}, \lambda_{2,k}^{(2)}, \lambda_{3,k}^{(2)})\\
&= Q_k^{(2)T} [\lambda_k^{(1)}]^{-1} Y_k Q_k^{(2)},
\end{aligned} \tag{18}$$

where $\lambda_{j,k}^{(2)}$ is the root of the secular equation $\det([\lambda_k^{(1)}]^{-1} Y_k(z) - \lambda\mathbf{I}) = 0$. Therefore, the transformation from generalized coordinates to canonical coordinates is given as

$$\begin{aligned}
X_k(\boldsymbol{r}) &= [Q_k^{(2)}]^{-1}[Q_k^{(1)}]^{-1} \begin{pmatrix} u_{x',k}(\boldsymbol{r}) \\ u_{z,k}(\boldsymbol{r}) \\ \psi_k(\boldsymbol{r}) \end{pmatrix}\\
&= U_{0,k}^\mathrm{c} \begin{pmatrix} x_{1,k}(z) \\ x_{2,k}(z) \\ x_{3,k}(z) \end{pmatrix} e^{-ikx'} + \mathrm{c.c.},
\end{aligned} \tag{19}$$

where $U_{0,k}^\mathrm{c}$ denotes the normalization constant of canonical coordinates, which is determined by the zero-point fluctuation of the SAW and will be discussed in Sec. III D.

Under the transformations $[Q_k^{(1)}]^{-1}$ and $[Q_k^{(2)}]^{-1}$, the kinetic and potential energy terms can be written in quadratic form. Correspondingly, the Lagrangian is given in canonical coordinates as

$$\mathcal{L} = \sum_{k>0} \int \frac{1}{2}\rho \left(\frac{\partial X_k}{\partial t}\right)^T \lambda_k^{\mathrm{K}} \left(\frac{\partial X_k}{\partial t}\right) dV - \sum_{k>0} \int \frac{1}{2} k^2 X_k^T \lambda_k^{\mathrm{P}} X_k \, dV. \tag{20}$$

Here, $X_k = (X_{1,k}, X_{2,k}, X_{3,k})^T$ denotes the canonical coordinate; $X_{j,k} = X_{j,k}^{(+)} + X_{j,k}^{(-)}$ is the component of the canonical coordinate, with the positive frequency term $X_{j,k}^{(+)} = U_{0,k}^{\mathrm{c}} x_{j,k}(z) e^{-i(kx'-\omega_k t)}$ and the negative frequency term $X_{j,k}^{(-)} = U_{0,k}^{\mathrm{c}} x_{j,k}(z) e^{i(kx'-\omega_k t)}$; and $\lambda_k^{\mathrm{K}} \equiv \mathrm{diag}(\lambda_{1,k}^{\mathrm{K}}, \lambda_{2,k}^{\mathrm{K}}, \lambda_{3,k}^{\mathrm{K}}) = Q_k^{(2)T} Y_k Q_k^{(2)}$ and $\lambda_k^{\mathrm{P}} \equiv \mathrm{diag}(\lambda_{1,k}^{\mathrm{P}}, \lambda_{2,k}^{\mathrm{P}}, \lambda_{3,k}^{\mathrm{P}}) = Q_k^{(2)T} Q_k^{(1)T} G_k(z) Q_k^{(1)} Q_k^{(2)}$ are the coefficient matrices. Thus, in terms of the canonical momentum $P_k = \partial\mathcal{L}/\partial(\partial X_k/\partial t)$, the Hamiltonian of a classical SAW is written as (see Sec. III of the Supplemental Material [62])

$$H_{\mathrm{SAW}} = \sum_{k>0}\sum_{j=1}^{3} \left[\lambda_{j,k}^{\mathrm{K}} \frac{P_{j,k}^2}{2M} + \lambda_{j,k}^{\mathrm{P}} \frac{Mk^2}{2\rho} X_{j,k}^2 \right], \tag{21}$$

with the mass $M = \int \rho \, dV$. Here, we point out that the above detailed expressions for quantization of a SAW are also applicable to Rayleigh-type SAWs in cubic piezomagnetic materials, whose nonzero components of the elastic, piezomagnetic, and magnetic permeability tensors are the same as (but different in detailed values from) those of terfenol-D shown in Table I.

C. Quantization condition

In the above discussion, we have derived the canonical coordinates, canonical momentum, and Hamiltonian of a classical SAW in a piezomagnetic waveguide. In this subsection, we will introduce the quantization condition to achieve the quantization of the SAW. We assume that the canonical coordinates $\hat{X}_k$ and the canonical momentum $\hat{P}_{k'}$ satisfy the communication relation $[\hat{X}_k, \hat{P}_{k'}] = i\hbar\delta_{kk'}$. By introducing the creation and annihilation operators $\hat{b}_k^\dagger = \hat{X}_{j,k}/(2X_{j,k}^{(+)}) - i\hat{P}_{j,k}/(2M\omega_k\lambda_{j,k}^{\mathrm{P}} X_{j,k}^{(+)})$ and $\hat{b}_k = \hat{X}_{j,k}/(2X_{j,k}^{(-)}) + i\hat{P}_{j,k}/(2M\omega_k\lambda_{j,k}^{\mathrm{P}} X_{j,k}^{(-)})$, one arrives at the canonical coordinate in quantization form as

$$\hat{X}_k = U_{0,k}^{\mathrm{c}} \begin{pmatrix} x_{1,k}(z) \\ x_{2,k}(z) \\ x_{3,k}(z) \end{pmatrix} \hat{b}_k^\dagger e^{-i(kx'-\omega_k t)} + \mathrm{H.c.} \tag{22}$$

Here, $\hat{b}_k^\dagger$ and $\hat{b}_k$ obey the standard bosonic commutation relations $[\hat{b}_k, \hat{b}_{k'}^\dagger] = \delta_{kk'}$ and $[\hat{b}_k, \hat{b}_{k'}] = [\hat{b}_k^\dagger, \hat{b}_{k'}^\dagger] = 0$. Correspondingly, we have the canonical momentum given in quantization form as

$$\hat{P}_k = \int i\omega_k \rho \, U_{0,k}^{\mathrm{c}} \begin{pmatrix} \lambda_{1,k}^{\mathrm{K}} x_{1,k}(z) \\ \lambda_{2,k}^{\mathrm{K}} x_{2,k}(z) \\ \lambda_{3,k}^{\mathrm{K}} x_{3,k}(z) \end{pmatrix} \times [\hat{b}_k^\dagger e^{-i(kx'-\omega_k t)} - \mathrm{H.c.}] \, dV. \tag{23}$$

Thus, the Hamiltonian of the SAW is written as

$$\hat{H}_{\mathrm{SAW}} = \sum_{k>0} \hbar\omega_k (\hat{b}_k^\dagger \hat{b}_k + \tfrac{1}{2}). \tag{24}$$

By taking the inverse transformation of canonical coordinates, i.e., $(\hat{u}_{x',k}(\boldsymbol{r}), \hat{u}_{z,k}(\boldsymbol{r}), \hat{\psi}_k(\boldsymbol{r}))^T = Q_k^{(1)} Q_k^{(2)} \hat{X}_k(\boldsymbol{r})$, we can obtain the generalized coordinates given in quantization form as

$$\begin{pmatrix} \hat{u}_{x'} \\ \hat{u}_z \\ \hat{\psi} \end{pmatrix} = \sum_{k>0} U_{0,k} \begin{pmatrix} U_{x',k}(z) \\ U_{z,k}(z) \\ \Psi_k(z) \end{pmatrix} \hat{b}_k e^{i(kx'-\omega_k t)} + \mathrm{H.c.} \tag{25}$$

with the coefficients $U_{x',k}(z)$, $U_{z,k}(z)$, and $\Psi_k(z)$ given as

$$\begin{aligned} U_{x',k}(z) &= 2e^{-kq_\alpha z}\cos(kq_\beta z + \theta), \\ U_{z,k}(z) &= -2i|\gamma| e^{-kq_\alpha z}\cos(kq_\beta z + \theta + \xi), \\ \Psi_k(z) &= i\frac{q_{33}}{\mu_{11}}[2Ae^{-kq_\alpha z}\cos(kq_\beta z + \theta + \tau) + A_3 e^{-kz}]. \end{aligned} \tag{26}$$

Here, the relation between the normalization constant $U_{0,k}$ of the generalized coordinates in Eq. (25) and the normalization constant $U_{0,k}^{\mathrm{c}}$ of canonical coordinates in Eq. (22) is determined by the coordinate transformation in Eq. (19). It is clear that Eq. (25) corresponds to the quantized traveling-wave SAW (propagating along the $+x'$ direction) in the waveguide. We note that the SAW resonator can be formed by fabricating two reflecting gratings on the surface of the piezomagnetic medium, and the corresponding quantization of the SAW in resonators can also be derived in a similar way as for the waveguide by considering the normalization condition.

D. Zero-point fluctuation of a quantized single-mode SAW

We know that the zero-point fluctuation of a quantized single-mode SAW play an important role in the study of the interaction between quantum systems and a quantized single-mode SAW via the magnetic field induced by the piezomagnetic effect. In analogy to cavity quantum electrodynamics [73], here we consider a semi-infinite box, with a finite lateral width L in the x'-y' plane and infinite length in the z direction, to determine the zero-point fluctuation of a quantized single-mode SAW. Thus, the normalization constant $U_{0,k}$ of generalized coordinates, which corresponds to the zero-point fluctuation of mechanical displacement, is determined by the energy of a single-mode SAW phonon. Following the coordinate transformation given in Eq. (19) and the generalized coordinates given in Eq. (25), one can determine the normalization constant $U^{c}_{0,k}$ of the canonical coordinate in Eq. (19) accordingly. Here, the expression of $U^{c}_{0,k}$ is not given since it is too complicated. In addition, it should be noted that the above method for determining the zero-point fluctuation is appropriate to arbitrary types of SAWs in general piezomagnetic materials.

Specially, for a Rayleigh-type SAW in the cubic piezomagnetic material terfenol-D (as given in Sec. II B), the corresponding normalization constant of generalized coordinates is calculated as $U_{0,k} \simeq (8.71 \times 10^{-22}/L)$ m^2 (see Sec. IV of the Supplemental Material [62]). Correspondingly, in terms of Eqs. (1), (25), and (26), the components of the induced magnetic field with wave number k at the surface ($z = 0$) are written in quantization form as (see Sec. IV of the Supplemental Material [62])

$$\hat{B}_{x',k}(z=0) = B^{\mathrm{zp}}_{x',k}\hat{b}_k e^{i(kx'-\omega_k t)} + \mathrm{H.c.}, \tag{27}$$

$$\hat{B}_{z,k}(z=0) = iB^{\mathrm{zp}}_{z,k}\hat{b}_k e^{i(kx'-\omega_k t)} + \mathrm{H.c.}, \tag{28}$$

where the corresponding zero-point fluctuations $B^{\mathrm{zp}}_{x',k}$ and $B^{\mathrm{zp}}_{z,k}$ are given as

$$B^{\mathrm{zp}}_{x',k} = 2kU_{0,k}q_{33}\left[A\cos(\theta+\tau) + \frac{A_3}{2}\right], \tag{29}$$

$$\begin{aligned} B^{\mathrm{zp}}_{z,k} &= 2kU_{0,k}q_{33}[q_\alpha|\gamma|\cos(\theta+\xi) + q_\beta|\gamma|\sin(\theta+\xi)] \\ &\quad + 2kU_{0,k}q_{33}[Aq_\alpha\cos(\theta+\tau) + Aq_\beta\sin(\theta+\tau)] \\ &\quad + 2kU_{0,k}q_{33}\left[\frac{q_{31}}{q_{33}}\cos(\theta) + \frac{A_3}{2}\right]. \end{aligned} \tag{30}$$

In Fig. 3, we give the zero-point fluctuations of the induced magnetic fields corresponding to a quantized single-mode SAW with wave number k versus the lateral width L and frequency ω_k of the SAW. Here, the lateral width L is taken to be $L = 1$–100 μm, which is within the width range of the SAW waveguide in existing research [74–76]. It is shown that a smaller lateral width L and higher frequency ω_k allow larger zero-point fluctuation of the magnetic field to be obtained, which would strengthen the coupling between quantum systems and a single-mode SAW via the magnetic field induced by the piezomagnetic effect. Specifically, we find that the zero-point fluctuation of magnetic fields can reach about 1 μT for $L = 1$ μm and $\omega_k/2\pi = 10$ GHz. In such a case, for a mechanical displacement that differs from the magnetic field by a factor kq_{ijk}, its corresponding zero-point fluctuation is about 1 fm.

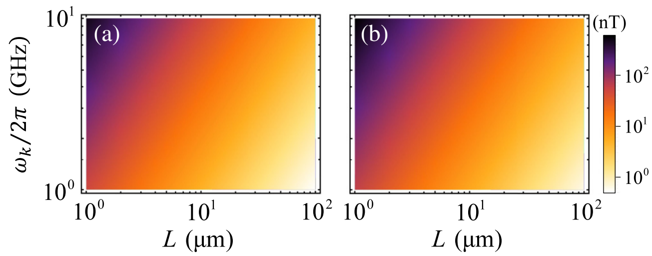

FIG. 3. The zero-point fluctuations (a) $B^{\mathrm{zp}}_{x',k}$ and (b) $B^{\mathrm{zp}}_{z,k}$ of the magnetic field induced by the piezomagnetic effect versus the lateral width L and the frequency ω_k of the SAW. Other parameters are the same as those in Fig. 2.

IV. COUPLING BETWEEN MAGNETIC QUANTUM SYSTEMS AND A QUANTIZED SINGLE-MODE SAW IN A PIEZOMAGNETIC WAVEGUIDE

In the above discussion, we have described a quantized SAW in a waveguide made of a piezomagnetic medium. Different from the SAW in a piezoelectric medium, the SAW in the piezomagnetic medium allows direct manipulations of magnetic quantum systems via the magnetic field induced by the piezomagnetic effect. A SAW is usually designed to operate in the frequency range from tens of megahertz to several gigahertz. We note that a superconducting circuit, ferromagnetic magnon, and defect center in diamond are typical solid-state magnetic quantum systems (with magnetic moments), which can operate within the domain of microwave frequency.

Without loss of generality, we now study the coupling between these quantum systems and a quantized single-mode SAW at the single-phonon level (i.e., the coupling between these quantum systems and a single-mode SAW phonon) in a piezomagnetic waveguide. Moreover, as schematically shown in Fig. 4(a), in order to excite the SAW in a waveguide [74–76] made of a piezomagnetic medium, an alternative way is to fabricate an interdigital transducer (IDT) on the piezomagnetic waveguide, with a layer of piezoelectric film deposited between the IDT and the piezomagnetic waveguide [53].

In the following study of this section, we take the quantized Rayleigh-type SAW in the cubic piezomagnetic material terfenol-D, which was described in Sec. III D, as an example to estimate the coupling strengths between these quantum systems and a quantized single-mode SAW. Here, we point out that these quantum systems can also be coupled with other types of SAWs in a general piezomagnetic medium.

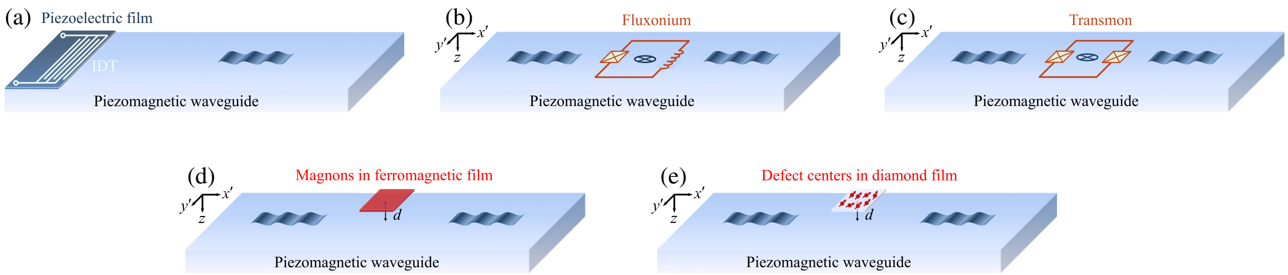

FIG. 4. (a) Schematic illustration for exciting a SAW in a piezomagnetic waveguide, where the IDT is fabricated on the piezomagnetic waveguide, with a layer of piezoelectric film deposited between the IDT and the piezomagnetic waveguide. (b)–(e) Schematic illustrations for coupling the (b) fluxonium qubit, (c) transmon qubit, (d) ferromagnetic magnon, and (e) defect center in diamond with the quantized SAW in a one-dimensional piezomagnetic waveguide via the magnetic field induced by the piezomagnetic effect. The superconducting qubits are deposited on the surface of the waveguide, while the ferromagnetic film and diamond film are suspended above the waveguide.

A. Superconducting qubit circuits and their couplings to the SAW

Superconducting qubit circuits based on Josephson junctions are macroscopic quantum systems, which have advantages such as flexibly designed and tunable system parameters, long decoherence time, as well as the capability of interfacing with other quantum systems [32–36,77,78]. It is well known that a superconducting qubit loop interrupted by Josephson junctions is very sensitive to the magnetic field [79–82]. We here take the fluxonium [83–86] and transmon [87–90] qubits as examples to study their couplings to a quantized single-mode SAW in a piezomagnetic waveguide via the magnetic field induced by the piezomagnetic effect.

1. Coupling of a quantized single-mode SAW to a fluxonium qubit

We first study the coupling between a fluxonium qubit and a quantized single-mode SAW in a piezomagnetic waveguide. As schematically shown in Fig. 4(b), the fluxonium qubit, which contains a superconducting loop interrupted by a Josephson junction and a big linear inductor, is coupled to the SAW via the magnetic field induced by the piezomagnetic effect. Thus, the Hamiltonian of the system (see Sec. V of the Supplemental Material [62]) in which the fluxonium qubit is coupled to a quantized single-mode SAW in the piezomagnetic waveguide is written as (hereafter, we take $\hbar = 1$ for simplicity)

$$H_{fx} = \omega_{fx}\hat{a}_{fx}^{\dagger}\hat{a}_{fx} - \frac{E_C}{12}(\hat{a}_{fx} + \hat{a}_{fx}^{\dagger})^4 + \omega_k\hat{b}_k^{\dagger}\hat{b}_k + (ig_{fx}\hat{a}_{fx}^{\dagger}\hat{b}_k + \text{H.c.}). \tag{31}$$

Here, $\omega_{fx} = 2\sqrt{2E_CE_L} + (E_J + E_L)\sqrt{E_C/2E_L}$ is the plasma-like frequency; $\hat{a}_{fx}^{\dagger}$ and $\hat{a}_{fx}$ are the creation and annihilation operators of the fluxonium qubit; $g_{fx} = -2\pi\sqrt[4]{2E_C/E_L}\,E_LB_{z,k}^{\text{zp}}S/\Phi_0$ is the coupling strength between the fluxonium qubit and a quantized single-mode SAW via the magnetic field induced by the piezomagnetic effect; E_C, E_J, and E_L denote the capacitive, Josephson, and inductive energies of the fluxonium qubit, respectively; Φ_0 is the magnetic flux quantum; $B_{z,k}^{\text{zp}}$ denotes the zero-point fluctuation of the induced magnetic field along the z direction as given in Eq. (30); and S denotes the effective loop area of the qubit that the induced magnetic field threads. Correspondingly, the transition frequency between the two lowest-energy states of the fluxonium qubit is given as $\omega_{10} = \omega_{fx} - E_C$. Equation (31) shows that the fluxonium qubit is linearly coupled to a quantized single-mode SAW in the waveguide via the magnetic field induced by the piezomagnetic effect.

2. Coupling of a quantized single-mode SAW to a transmon qubit

We now study the coupling between a transmon qubit and a quantized single-mode SAW in a piezomagnetic waveguide. As schematically shown in Fig. 4(c), the transmon qubit, which contains a superconducting loop interrupted by two Josephson junctions, is coupled to the SAW via the magnetic field induced by the piezomagnetic effect. Thus, the Hamiltonian of the system (see Sec. VI of the Supplemental Material [62]) in which the transmon qubit is coupled to a quantized single-mode SAW in the piezomagnetic waveguide is given as

$$H_{ts} = \omega_{ts}\hat{a}_{ts}^{\dagger}\hat{a}_{ts} - \frac{E_C}{12}(\hat{a}_{ts} + \hat{a}_{ts}^{\dagger})^4 + \omega_k\hat{b}_k^{\dagger}\hat{b}_k + g_{ts}(\hat{a}_{ts} + \hat{a}_{ts}^{\dagger})^2(\hat{b}_k - \hat{b}_k^{\dagger})^2. \tag{32}$$

Here, $\omega_{ts} = 4\sqrt{E_CE_J}$ denotes the Josephson plasma frequency; $\hat{a}_{ts}^{\dagger}$ and $\hat{a}_{ts}$ are the creation and annihilation operators of the transmon qubit; the parameter $g_{ts} = -2\pi\sqrt{E_CE_J}(\pi B_{z,k}^{\text{zp}}S)^2/2\Phi_0^2$ is the coupling strength between the transmon qubit and a quantized single-mode SAW via the magnetic field induced by the piezomagnetic effect; and E_C, E_J, and E_L denote the capacitive, Josephson, and inductive energies of the transmon qubit, respectively. Correspondingly, the transition frequency between the two lowest-energy states of the transmon qubit is given as $\omega_{10} = \omega_{ts} - E_C$. Equation (32) shows that, different from the fluxonium qubit, the transmon qubit is quadratically coupled to a quantized single-mode SAW via the magnetic field induced by the piezomagnetic effect.

3. Coupling strength between a quantized single-mode SAW and superconducting qubits

In Figs. 5(a) and 5(b), we choose different lateral widths L to display the coupling strengths in Eqs. (31) and (32) of the fluxonium and transmon qubits with a quantized single-mode SAW versus the loop area S of the qubit. Here, the frequency of the SAW is taken to be resonant with the transition frequency between the two lowest-energy states of the fluxonium and transmon qubits in Figs. 5(a) and 5(b), respectively. It is found that, with the decrease of L or the increase of S, the coupling strength can be enhanced significantly. Therefore, in the case of superconducting qubits that are coupled to a single-mode SAW via the magnetic field, designing phononic devices with small lateral widths or qubit circuits with large loop areas would be necessary to achieve strong coupling strength.

Furthermore, we point out that, besides the linear coupling, a single-mode SAW in a piezomagnetic waveguide can interact with a superconducting qubit via quadratic coupling. This is different from the quantized single-mode SAW in a piezoelectric waveguide, which typically interacts with a superconducting qubit via linear coupling. In the present models, the linear coupling or quadratic coupling arises from the intrinsic properties of the qubits. Thus, when resorting to a specially designed superconducting qubit circuit, one could enable the interaction between the qubits and SAW via other types of nonlinear couplings. This would enable more potential applications in quantum sensing, quantum communication, and quantum computing, e.g., precision measurement [91,92], quantum gates [93,94], generation of nonclassical states [95,96], mechanical cooling [97,98], and parametric conversion [99,100].

In the above study, we simply assume that the effect of the magnetic field induced by the SAW on the superconductivity of the superconducting qubit is negligibly small. And also, the superconducting qubit might be coupled to the SAW in the piezomagnetic waveguide through flip-chip bonding technology [37,101,102] to minimize the effect of the piezomagnetic waveguide on the superconductivity and coherence of the qubit. Correspondingly, for a distance d between the superconducting qubit and the surface of the piezomagnetic waveguide, the coupling strength between the fluxonium (transmon) qubit and a quantized single-mode SAW reduces to $g_{fx}e^{-kd}$ ($g_{ts}e^{-kd}$). That means that the presence of the distance d would lead to variation of the coupling strength between the qubit and the SAW, as shown in Figs. 5(c) and 5(d). Generally, a large distance corresponds to weaker coupling for a given qubit. For different qubits, their coupling strengths with the SAW are different even if the distance d is the same. For example, it is found that, with the increase of d, the coupling strength between the transmon qubit and the SAW decreases more rapidly, as compared with that between the fluxonium qubit and the SAW.

B. Coupling of a quantized single-mode SAW to ferromagnetic magnons

The magnon [103,104] is the spin-wave quantum in magnetically ordered systems. A ferromagnet, which is a typical example of a magnetically ordered system, is well known for its rich properties, e.g., large magnetization, long decoherence time, magnetostriction, and nonlinearity [103–112]. These properties mean that ferromagnetic magnons have promising applications in quantum sensors, quantum communication, and quantum transduction [50–53,104,109]. Here, we study the interaction between ferromagnetic magnons and a quantized single-mode SAW in a piezomagnetic waveguide.

Note that the magnetic potential of SAW decays exponentially in the space above a waveguide made of a piezomagnetic medium. To achieve coupling between the ferromagnetic magnon and a quantized single-mode SAW in a waveguide via the magnetic field induced by the piezomagnetic effect, we consider the system composed of a piezomagnetic waveguide and a ferromagnetic film suspended above the waveguide, as schematically shown in Fig. 4(d). Here, we focus on the case of low excitation for a large number N of ferromagnetic spins, that is, the mean excitation number of spins is much smaller than the total number of spins [104]. Then, the interaction Hamiltonian, between a single Kittel-mode magnon (generated via spatially uniform magnetization of spins) [104,106] and a quantized single-mode SAW in the piezomagnetic waveguide, is written as (see Sec. VII of the Supplemental Material [62])

$$H_{fm} = g_{fm}\hat{m}^{\dagger}\hat{b}_k + \text{H.c.} \tag{33}$$

Here, $g_{fm} = (1-i)\sqrt{N}\gamma_f B^{\text{zp}}_{x',k}e^{-kd}/2\sqrt{2}$ denotes the coupling strength between a single Kittel-mode magnon and a quantized single-mode SAW via the magnetic field induced by the piezomagnetic effect; γ_f is the gyromagnetic ratio; d is the distance between the film and the surface of the waveguide; and $\hat{m}^{\dagger}$ and $\hat{m}$ are the creation and annihilation operators of the magnon. As shown in Fig. 5(e), for the typical ferromagnetic material nickel with operation frequency $\omega_f/2\pi = 3$ GHz and gyromagnetic ratio $\gamma_f/2\pi \simeq 30.59$ GHz [105], when we take the

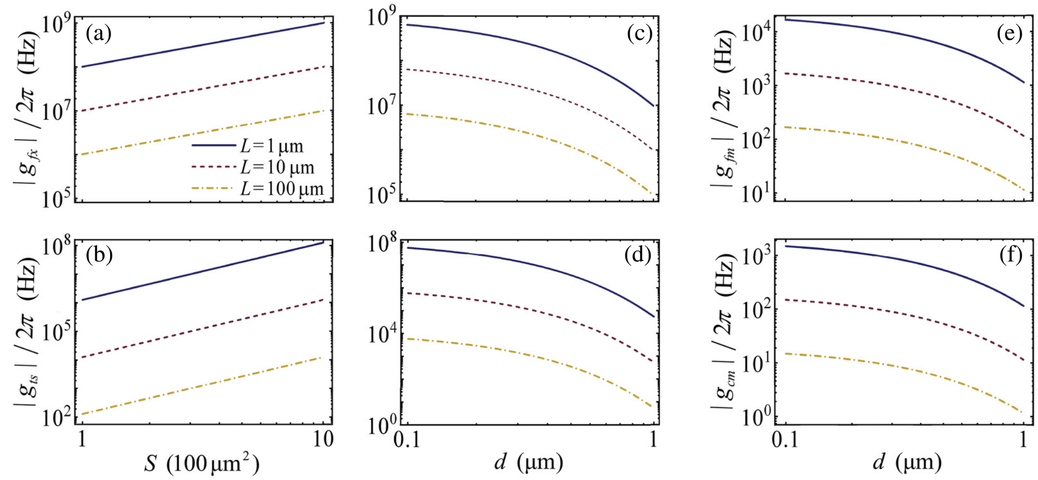

FIG. 5. (a),(c) The coupling strength between the fluxonium qubit and a quantized single-mode SAW via the magnetic field induced by the piezomagnetic effect versus (a) the loop area S or (c) the distance d for different lateral widths L. (b),(d) The coupling strength between the transmon qubit and a quantized single-mode SAW via the magnetic field induced by the piezomagnetic effect versus (b) the loop area S or (d) the distance d for different lateral widths L. (e),(f) The coupling strength between (e) a single ferromagnetic Kittel-mode magnon or (f) a defect center and a quantized single-mode SAW via the magnetic field induced by the piezomagnetic effect versus the distance d for different lateral widths L. The parameters are chosen as follows. (a),(c) Fluxonium: $E_C/2\pi = E_L/2\pi = 1$ GHz, $E_J/2\pi = 3$ GHz, $\omega_k/2\pi = 4.66$ GHz, and (a) $d = 0$ and (c) $S = 1000\ \mu\text{m}^2$. (b),(d) Transmon: $E_C/2\pi = 100$ MHz, $E_J/2\pi = 10$ GHz, $\omega_k/2\pi = 3.9$ GHz, and (b) $d = 0$ and (d) $S = 1000\ \mu\text{m}^2$. (e) Ferromagnetic magnon: $\gamma_f/2\pi = 30.59$ GHz, $\omega_k/2\pi = 3$ GHz, and $N = 100$. (f) Defect center: $\gamma_c/2\pi = 28$ GHz and $\omega_k/2\pi = 2.87$ GHz. Other parameters are the same as those in Fig. 2.

distance $d = 0.1\ \mu$m, lateral width $L = 1\ \mu$m, and spin number $N = 100$, the coupling strength between a single Kittel-mode magnon and a quantized single-mode SAW with frequency $\omega_k = \omega_f$ is estimated as $|g_{fm}|/2\pi \simeq 16.73$ kHz. The results indicate that a smaller lateral width L for the SAW device and a smaller distance d between the SAW device and the ferromagnetic film would contribute to achieve strong coupling strength.

Additionally, we note that when the ferromagnetic film is deposited on the surface of an elastic medium, the propagation of a SAW through the film would generate elastic strain, allowing one to drive the magnetization dynamics of the ferromagnetic magnons via the magnetoelastic interaction [50–53]. Here, it is found that, when the ferromagnetic magnons are coupled to SAW via the strain induced by the piezomagnetic effect, one can achieve the interaction between ferromagnetic magnons and the SAW via both linear and nonlinear magnetomechanical couplings simultaneously (see Sec. VII of the Supplemental Material [62]). This would offer promising applications in quantum sensing [113,114] and storage of quantum information [115,116].

Moreover, the above discussion focuses on the coupling between ferromagnetic magnons and a SAW via the magnetic field or the strain induced by the piezomagnetic effect. We point out that, in a model consisting of ferromagnetic and piezomagnetic materials, the interlayer exchange coupling [117–119] that arises from the interaction between two spins in two different layers of magnetic materials may also contribute to the coupling between the ferromagnetic magnons and the SAW in the piezomagnetic medium. This type of coupling has been widely used in nonreciprocal transmission [120,121], tailored magnon-phonon coupling [122,123], and magnetic memory [124,125]. Therefore, the use of interlayer exchange coupling would enable further development of our present magnon-phonon quantum system.

C. Coupling of a quantized single-mode SAW to defect centers in diamond

The defect center in diamond [126], which is considered as a spin, can operate at room temperature and has long decoherence time. Thus, it provides a promising platform for quantum memory, quantum communication, and quantum sensors [26–28,72,126–131]. Different from previous studies involving the interaction between electromagnetic fields at telecommunication wavelength [128–130] or SAWs in a piezoelectric medium [26–28], here we focus on the domain of microwave frequency to study the coupling between defect centers and SAW in a piezomagnetic medium.

Similarly, the coupling between defect centers and SAW can be realized via the magnetic field induced by the piezomagnetic effect. As schematically shown in Fig. 4(e), we consider the system composed of a piezomagnetic waveguide and the defect centers contained in a diamond film that is suspended above the waveguide. Correspondingly, the interaction Hamiltonian in which a single defect center is coupled to a quantized single-mode SAW in the piezomagnetic waveguide is written as (see Sec. VIII of the Supplemental Material [62])

$$H_{cm} = g_{cm}\sigma_+\hat{b}_k + \text{H.c.} \tag{34}$$

Here, $g_{cm} = (1-i)\gamma_c B^{\text{zp}}_{x',k} e^{-kd}/2\sqrt{2}$ is the coupling strength between the single defect center and a quantized single-mode SAW, with the gyromagnetic ratio of defect center γ_c; and σ_+ and σ_- are the ladder operators of the defect center. Typically, for the nitrogen-vacancy (N-V) center with transition frequency $\omega_c/2\pi = 2.87$ GHz and gyromagnetic ratio $\gamma_c/2\pi \simeq 28$ GHz [126], when we take $L = 1$ μm and $d = 0.1$ μm, the coupling strength between a single N-V center and a single-mode SAW phonon with frequency $\omega_k = \omega_c$ is about $|g_{cm}|/2\pi \simeq 1484$ Hz, as shown in Fig. 5(f). Similar to the case of the coupling between a ferromagnetic magnon and a SAW, smaller lateral width L for the SAW device and smaller distance d between the SAW device and the defect center would be better to obtain strong coupling strength.

Moreover, we note that, besides the electric and magnetic fields, the defect centers can be controlled via strain using electromechanical or optomechanical systems [132–136]. Thus, in our present model, when the diamond film is deposited on the surface of a piezomagnetic waveguide, one can manipulate the defect centers using the SAW via both the magnetic field and the strain induced by the piezomagnetic effect (see Sec. VIII of the Supplemental Material [62]). Specifically, for the typical strain-driven N-V center [132], its maximum coupling strength with a SAW via the induced strain is estimated as $g_{cs}/2\pi \sim 100$ Hz for a lateral width $L = 1$ μm. That means that the coupling strength of the N-V center with the strain is much smaller than its coupling strength with the magnetic field, which is in agreement with previous studies [13,131].

D. Discussions about coupling strengths

In the above, we have studied the coupling between solid-state magnetic quantum systems (i.e., superconducting qubit, ferromagnetic magnon, and defect center in diamond) and a single-mode SAW phonon in a waveguide made of a piezomagnetic medium. We note that for these systems used as qubits, each of them has its own features, and their couplings to the SAW phonon are also different from each other. For comparison, we summarize the operating temperature, operating frequency, coupling type, decoherence rate, and coupling strength to the single-mode SAW phonon via the magnetic field in Table II.

The superconducting qubit, which operates at low temperature ($\sim$ 10 mK), can interact strongly with the single-mode SAW phonon since the coupling strength ($\sim$ 0.01 Hz–100 MHz) can be stronger compared to the decoherence rate ($\sim$ 0.01 MHz). Thus, a SAW in the piezomagnetic medium offers an alternative way for the individual manipulation of superconducting qubits via the magnetic field induced by the piezomagnetic effect. In contrast, compared with the superconducting qubit, the ferromagnetic magnon and defect center have smaller decoherence rates ($\sim$ 1 Hz–10 kHz) and operate at higher temperature ($\sim$ 1–300 K). However, a sample of ferromagnetic materials with high spin density [53,105,111] (or a sample of diamond with many defect centers [28,134,137,138]) is required to achieve coherent manipulation of these collective spins. Besides the magnetic field, the ferromagnetic magnons (or defect centers in diamond) can interact with the SAW via the strain induced by the piezomagnetic effect. Therefore, a SAW in a piezomagnetic medium provides an alternative way for the manipulation of ferromagnetic magnons or defect centers via the magnetic field or strain induced by the piezomagnetic effect.

We would like to point out that the above studies focus on the case of a traveling-wave SAW in a waveguide, whose amplitude is uniform in space. Thus, the corresponding coupling strength is independent of the locations of the magnetic quantum systems. However, in the case of a standing-wave SAW in a resonator, which will be studied in our future work, the amplitude of the SAW is space-dependent, and thus the coupling strengths of the magnetic quantum systems to the SAW are also space-dependent. We also note that the wavelength of the SAW ($\sim$ 1 μm in our present studies) is comparable to the size of a single superconducting qubit ($\sim$ 1–100 μm) [32–36] or a sample ($\sim$ 10–100 μm) containing many ferromagnetic spins [53,105,111] or defect centers [28,134,137,138]. Therefore, these magnetic quantum systems cannot be considered as point particles when they are coupled to a SAW in a piezomagnetic resonator.

V. QUBIT- QUBIT INTERACTION MEDIATED BY A MULTIMODE SAW PHONON IN A PIEZOMAGNETIC WAVEGUIDE

In the previous section, we studied the couplings between several typical magnetic quantum systems and a single-mode SAW phonon in a piezomagnetic waveguide. In fact, when a magnetic quantum system is coupled to a SAW in a waveguide, it would simultaneously interact with multiple modes of SAW phonons in the waveguide. In this section, by taking into account a quantized Rayleigh-type SAW in the cubic piezomagnetic material terfenol-D (described in Sec. III D) and the superconducting fluxonium qubit as examples, we further study the distant interaction between two identical qubits mediated by multimode SAW phonons in a piezomagnetic waveguide. In the following study, the transition frequencies ω_{10} of the two qubits are taken as $\omega_{10}/2\pi = 4.66$ GHz according to the parameters of Fig. 5(b). To characterize

TABLE II. Basic properties of typical magnetic quantum systems [34–36,78,104,105,126,131], along with comparisons of coupling strengths between these systems and a quantized single-mode SAW in a piezomagnetic waveguide. Other parameters are the same as those in Figs. 2 and 5 except $L = 1$–$100\ \mu$m, $S = 100$–$1000\ \mu\text{m}^2$, and $d = 0.1$–$1\ \mu$m.

Qubits	Fluxonium	Transmon	Nickel for ferromagnetic magnon	N-V center for defect center
Operating temperature	~ 10 mK	~ 10 mK	from ~ 1 K to room temperature	room temperature
Operating frequency $\omega/2\pi$	1–5 GHz	1–5 GHz	0.1–5 GHz	1–5 GHz
Coupling type	either electric or magnetic	either electric or magnetic	either magnetic or strain	either electric, magnetic, or strain
Decoherence rate $\Gamma/2\pi$ of single qubit	~ 0.01 MHz	~ 0.01 MHz	~ 1 kHz–10 kHz	~ 1 Hz–1 kHz
Coupling strength $g/2\pi$ between single qubit and SAW (in waveguide) via magnetic field	~ 10 kHz–100 MHz	~ 0.01 Hz–10 MHz	~ 10 Hz–10 kHz	~ 1 Hz–1 kHz

such interaction, we focus on the dynamical evolutions of population and entanglement of the two qubits.

A. Dynamical equations of population and concurrence

As schematically shown in Fig. 6, the SAW phonons in a one-dimensional waveguide are coupled to two superconducting fluxonium qubits at positions $x' = x'_a$ and $x' = x'_b$, respectively. Here we focus on the single-excitation properties of the system. Thus the evolutions of the two qubits are given as (see Sec. IX of the Supplemental Material [62])

$$\frac{\partial}{\partial t}\alpha_A(t) = -\Gamma_0\alpha_A(t) - \Gamma_0 e^{i\theta_{\mathbb{T}}}\alpha_B(t-\mathbb{T})\Theta(t-\mathbb{T}), \quad (35)$$

$$\frac{\partial}{\partial t}\alpha_B(t) = -\Gamma_0\alpha_B(t) - \Gamma_0 e^{i\theta_{\mathbb{T}}}\alpha_A(t-\mathbb{T})\Theta(t-\mathbb{T}), \quad (36)$$

where $\alpha_A(t)$ and $\alpha_B(t)$ are the probability amplitudes of the qubit A and qubit B, which are excited to their first-excited states $|1\rangle_A$ and $|1\rangle_B$ by the SAW phonons. The parameter $\theta_{\mathbb{T}} = \omega_{10}\mathbb{T}$ represents the phase that results from the propagation of the SAW, with the transition frequency ω_{10} between two lowest-energy states of each qubit and the delay time $\mathbb{T} = |x'_b - x'_a|/v$ between the two qubits. In addition, $\Theta(t-\mathbb{T})$ is the Heaviside step function; and Γ_0 is the decay rate from the qubit to the SAW waveguide,

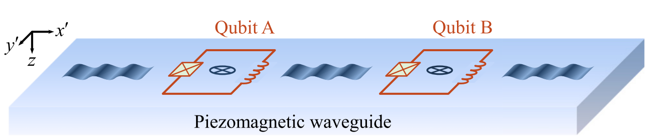

FIG. 6. Schematic illustration for coupling two distant superconducting fluxonium qubits mediated by multimode SAW phonons in a one-dimensional waveguide via the magnetic field induced by the piezomagnetic effect.

while other decay rates of the qubit have been neglected. Thus, the population evolutions of the two qubits are calculated as $P_A(t) = |\alpha_A(t)|^2$ and $P_B(t) = |\alpha_B(t)|^2$. Equations (35) and (36) also show that the SAW waveguide results in decays of the two qubits and induces the interaction between the two qubits.

To quantify the entanglement of the two qubits, here we resort to the concurrence [139,140], derived from the reduced density matrix in the basis $\{|1_A, 1_B\rangle, |1_A, 0_B\rangle, |0_A, 1_B\rangle, |0_A, 0_B\rangle\}$. Thus, the time evolution of the concurrence $C(t)$ is given as (see Sec. IX of the Supplemental Material [62])

$$C(t) = 2|\alpha_A(t)\alpha_B(t)^*|, \quad (37)$$

where the probability amplitudes $\alpha_A(t)$ and $\alpha^*_B(t)$ are obtained by solving the dynamical equations (35) and (36).

B. Time-delay interaction of two qubits

In the present model, the time-delay effect due to the propagation of the SAW in the waveguide is essential in the interaction between the two qubits. Thus, we first choose different delay times $\mathbb{T}$ to study the population evolutions of the two qubits in Fig. 7. In the following discussion, we consider the initial condition that the qubit A (qubit B) is in the excited (ground) state. As shown in Fig. 7(a), at the time $0 \leq t < \mathbb{T}$, qubit A decays exponentially, while qubit B remains in the ground state. This is because the SAW phonons, generated by the decay of qubit A, have not yet propagated to the position of qubit B. At the time $\mathbb{T} \leq t < 2\mathbb{T}$, qubit B is excited and then decays exponentially, while qubit A remains in the ground state. This can be interpreted as follows: qubit B is excited by the SAW phonons generated by qubit A, but the SAW phonons generated by the decay of qubit B have not yet propagated to qubit A due to the delay time. As time t goes on, more energy is transferred to the SAW phonons

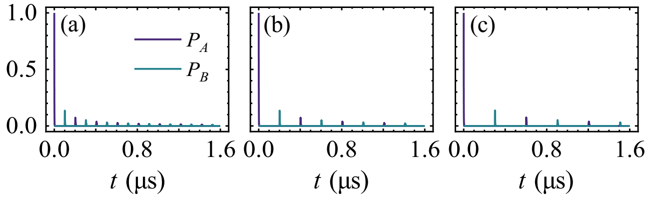

FIG. 7. The population evolution of the two qubits when the delay time is taken as (a) $\mathbb{T} = 0.1$ μs, (b) $\mathbb{T} = 0.2$ μs, and (c) $\mathbb{T} = 0.3$ μs. Other parameters are $\omega_{10}/2\pi = 4.66$ GHz and $\Gamma_0/2\pi = 100$ MHz.

in the waveguide, which ultimately leads to the decay of time-delay Rabi oscillation between the two qubits. Here, we note that, with the increase of the delay time $\mathbb{T}$, the time required for SAW phonons to propagate between the two qubits is increased accordingly, and thus the decay of Rabi oscillation becomes slower, as shown in Figs. 7(b) and 7(c).

In addition to the delay time, the decay rate Γ_0 of the qubit also plays a crucial role in the population evolutions of the two qubits. This is primarily because the decay rate Γ_0 determines the time for the energy to be transferred from the qubit to the SAW phonons in the waveguide. We show the population evolutions of the two qubits for different decay rate Γ_0 in Fig. 8. In the case of $\Gamma_0^{-1} \ll \mathbb{T}$, as shown in Fig. 8(a), the decay time of the qubit is much less than the delay time. Thus, before the SAW phonons generated by qubit A (qubit B) propagate to qubit B (qubit A), qubit A (qubit B) decays rapidly to the waveguide. As the decay rate decreases, e.g., $\Gamma_0^{-1} = \mathbb{T}$, as shown in Fig. 8(b), the decay of the qubit becomes slower. Thus, before qubit A (qubit B) decays completely to the waveguide, qubit B (qubit A) is excited by the SAW phonons that are generated by qubit A (qubit B). Specifically, in the case of $\Gamma_0^{-1} \gg \mathbb{T}$, as shown in Fig. 8(c), the decay time of the qubit is much larger than the delay time. In such a case, before qubit A (qubit B) decays completely to the waveguide, the phonons generated by qubit A (qubit B) would be partly reflected back to qubit A (qubit B) by qubit B (qubit A). The reflected phonons interfere with the phonons generated by the decay of the qubit, which ultimately results in a portion of the energy being trapped within the two qubits.

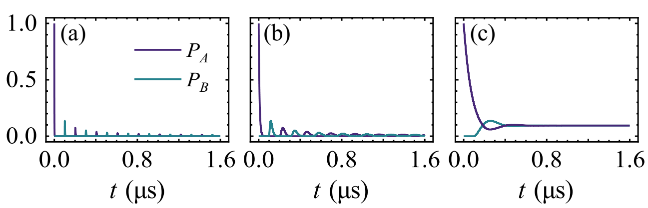

FIG. 8. The population evolution of the two qubits when the decay rate to the SAW waveguide is taken as (a) $\Gamma_0/2\pi = 100$ MHz, (b) $\Gamma_0/2\pi = 10$ MHz, and (c) $\Gamma_0/2\pi = 1$ MHz. Other parameters are the same as those in Fig. 7 except $\mathbb{T} = 0.1$ μs.

From Fig. 8(c), one can see that the decay of the two qubits to the waveguide is highly dependent on the interference between the phonons generated by qubit A (qubit B) and the phonons reflected by qubit B (qubit A). As shown in Eqs. (35) and (36), such interference is determined by the phase $\theta_T = \omega_{10}\mathbb{T}$ with a period π. When the transition frequency ω_{10} of the qubit is given, the interference is determined by the delay time $\mathbb{T}$. To clearly illustrate such interference, we study the population evolutions of the two qubits for different phase $\theta_{\mathbb{T}}$ for given frequency $\omega_{10}/2\pi = 4.66$ GHz under the condition $\Gamma_0^{-1} \gg \mathbb{T} = \theta_T/\omega_{10}$, i.e., the decay time of the qubit is much longer than the delay time.

When qubit A (qubit B) decays into the waveguide, qubit B (qubit A) can be considered as a mirror [35,141–143], which leads to the standing wave for the SAW phonon with frequency $\omega_k = \omega_{10}$. For the phase $\theta_{\mathbb{T}} = \pi/2$, as shown in Fig. 9(a), each qubit is located at the antinode of the standing wave [141–143], which results in the enhancement of the decay of the qubit to the waveguide. As the phase $\theta_{\mathbb{T}}$ varies from $\pi/2$ to π, each qubit is no longer located at the antinode of the standing wave, and thus the decay of the qubit becomes slower, with, for example, $\theta_{\mathbb{T}} = 3\pi/4$, as shown in Fig. 9(b). Specifically, for the phase $\theta_{\mathbb{T}} = \pi$, as shown in Fig. 9(c), each qubit is located at the node of the standing wave [141–143], which leads to the suppression of the decay of the qubit to the waveguide.

Moreover, we point out that the phase $\theta_{\mathbb{T}} = \omega_{10}\mathbb{T}$ with period π would also have an effect on the entanglement of the two qubits. In Fig. 10, we still focus on the condition $\Gamma_0^{-1} \gg \mathbb{T}$ and choose different phase $\theta_{\mathbb{T}}$ to show the evolution of the concurrence with time t for given frequency $\omega_{10}/2\pi = 4.66$ GHz. It is shown that the entanglement of the two qubits reaches a maximum $C \simeq 0.2$ rapidly when both qubits are excited at time t with $\mathbb{T} < t < 2\mathbb{T} < \Gamma_0^{-1}$ with given frequency $\omega_{10}/2\pi = 4.66$ GHz. When the phase θ_T is taken as $\theta_T = \pi/2$, as considered in Fig. 9(a), the enhanced decay of the qubit would lead

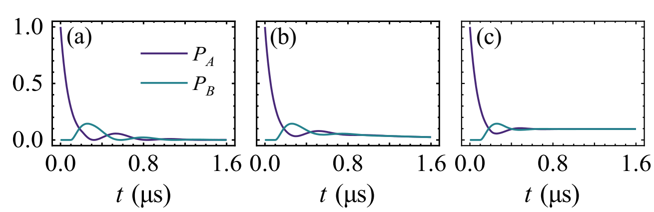

FIG. 9. The population evolution of the two qubits when the relative phase between the two qubits is taken as (a) $\theta_{\mathbb{T}} = \pi/2$, (b) $\theta_{\mathbb{T}} = 3\pi/4$, and (c) $\theta_{\mathbb{T}} = \pi$. Other parameters are the same as those in Fig. 7 except $\mathbb{T} = 0.1$ μs + mod$(\theta_{\mathbb{T}}, \pi)/\omega_{10}$ and $\Gamma_0/2\pi = 1$ MHz, with mod$(\theta_{\mathbb{T}}, \pi)$ denoting the remainder of $\theta_{\mathbb{T}}$ divided by π.

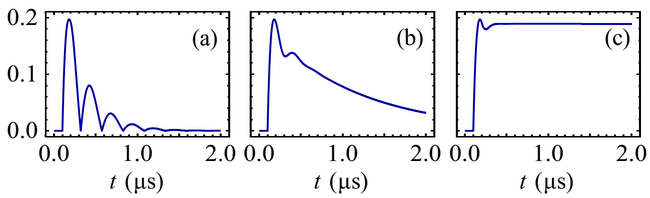

FIG. 10. The concurrence of the two qubits when the relative phase between the two qubits is taken (a) $\theta_{\mathbb{T}} = \pi/2$, (b) $\theta_{\mathbb{T}} = 3\pi/4$, and (c) $\theta_{\mathbb{T}} = \pi$. Other parameters are the same as those in Fig. 9.

to the rapid disentanglement of the two qubits, as shown in Fig. 10(a). When the phase $\theta_{\mathbb{T}}$ varies from $\pi/2$ to π, the enhancement of the decay of the qubit is modified, and thus the decay from entanglement to disentanglement becomes slower, as shown in Fig. 10(b) with, for example, $\theta_T = 3\pi/4$ as considered in Fig. 9(b). In particular, when the phase $\theta_{\mathbb{T}}$ is taken as $\theta_{\mathbb{T}} = \pi$, as considered in Fig. 9(c), the suppressed decay of the qubit would ultimately result in steady entanglement with the concurrence $C \simeq 0.19$, as shown in Fig. 10(c).

VI. DISCUSSION

In our present models, the magnetic quantum systems used as qubits (e.g., N-V center, magnon, and various superconducting qubits) are coupled to the SAW phonons via the magnetic field or stain induced by the piezomagnetic effect, and thus the information on SAW phonons can be detected by the qubits. That means that, when external disturbances (e.g., magnetic field, strain, or temperature) are applied to the piezomagnetic medium, one could realize qubit-mediated sensors with SAW phonons in the piezomagnetic medium. By controlling the interaction between the qubits and the SAW phonons, one can prepare various nonclassical states (e.g., squeezed state or entangled state) of the SAW phonons to achieve precision measurement. Therefore, our studies would provide new ways for quantized SAW-based sensing.

Furthermore, besides the magnetic quantum systems discussed in our present studies, a quantized SAW in a piezomagnetic medium can also be coupled to other quantum systems, such as quantum dots [29–31], chiral molecules [144,145], and waveguides [74,146,147]. Thus, a quantized SAW in a piezomagnetic medium provides an alternative way for the integration of different quantum systems, and may have potential applications in quantum communication and quantum computing.

Generally, in a magnetomechanical material that involves coupling between magnetic field and mechanical vibration [148–151], there exists not only the (linear) piezomagnetic effect, which dominates in the case of a weak driving field, but also the (second-order nonlinear) magnetostrictive effect, which becomes significant in the case of a strong driving field. In our present study, we focus on the case of a weak driving field and assume that the magnetostrictive effect is negligibly small. Thus, our discussions are limited to linear piezomagnetic coupling, and the derivations are based on the linear constitutive equations in a piezomagnetic medium with negligibly small magnetostrictive effect.

However, in the case of a strong driving field, the discussions should consider both the linear piezomagnetic coupling and nonlinear magnetostrictive coupling, and the derivations require the nonlinear constitutive equations [148] in a general magnetomechanical medium with both piezomagnetic and magnetostrictive effects. In such a case, depending on the intrinsic properties of the material, crystal orientation, and external perturbations (e.g., magnetic field), the simultaneously present piezomagnetic and magnetostrictive effects could enhance or counteract each other [149–151]. This would lead to the enhancement or reduction of the magnetic field and mechanical vibration, and thus has applications in signal processing [152–155]. Therefore, the generation of SAWs under both the piezomagnetic and magnetostrictive effects, as well as the couplings between a SAW and quantum systems via these two effects, is also an important and interesting issue, which will be further studied in our future work.

Additionally, we would like to remark that our present study is limited to linear piezomagnetic coupling. Thus, we take terfenol-D, which is considered as a piezomagnetic material (under a weak driving field) in many theoretical and experimental studies [65,68–72], as an example to derive more detailed expressions on the quantum theory of SAWs in a piezomagnetic medium, e.g., the approximate value of the zero-point fluctuation for the SAW and the coupling strengths of the SAW to several magnetic systems. However, detailed expressions for the quantized SAW in other piezomagnetic materials, e.g., uranium dioxide [149], can also be derived with the given material parameters.

We would also like to emphasize that we study an ideal case where all dampings of SAW phonons are neglected. In practice, both acoustic and magnetic dampings [156–158] are important to the propagation of SAW phonons in a piezomagnetic waveguide. We note that the damping of the piezomagnetic material terfenol-D, which depends on the external perturbation [159–161], is usually considered to be large [162–164]. Thus, in order to ensure a SAW propagating free from damping over a chip-scale distance, a piezomagnetic material with low damping (perhaps yttrium iron garnet, Mn_3Sn, or uranium dioxide) would be a better choice for the fabrication of the waveguide. We also mention that these damping effects on the SAW can be theoretically resolved according to quantum theory [165,166] by introducing external degrees of freedom, which are coupled to the SAW.

VII. CONCLUSIONS

In conclusion, we have studied the quantum theory of SAWs in a piezomagnetic medium by resorting to the canonical quantization method. Based on the theory of the classical SAW, which is obtained by solving the wave equation in a general piezomagnetic medium, we derive the Hamiltonian of the quantized SAW in a strip waveguide made of a piezomagnetic medium, and give the quantization expressions for the mechanical displacement and magnetic field induced by the piezomagnetic effect. Based on this, we study the interaction between several typical magnetic quantum systems (i.e., superconducting qubits, ferromagnetic magnons, and defect centers in diamond) and a quantized single-mode SAW in a piezomagnetic waveguide at the single-phonon level. It is found that the intrinsic properties of a SAW in a piezomagnetic medium enable it to interact with these magnetic systems via the magnetic field or strain induced by the piezomagnetic effect. This is very different from the SAW in a piezoelectric medium, which is coupled to quantum systems via the electric field or strain induced by the piezoelectric effect.

Furthermore, we study the interaction between two qubits mediated by multimode SAW phonons in a piezomagnetic waveguide. The results show that the interaction between two qubits depends strongly on the delay time, the decay of the qubit, and the phase due to the propagation of the SAW between the two qubits via the waveguide. This leads to the time-delay Rabi oscillation, energy trapping within the qubits, and steady entanglement between the two qubits. We mention that the coupling strength between the magnetic quantum systems and the quantized single-mode SAW in the piezomagnetic waveguide is not strong at the single-phonon level. To achieve strong coupling, a SAW resonator fabricated on the surface of the piezomagnetic medium needs to be further explored.

ACKNOWLEDGMENTS

This work was supported by the National Natural Science Foundation of China with Grants No. 12374483, No. 92365209, and No. 62474012.

[1] S. Datta, *Surface Acoustic Wave Devices* (Prentice-Hall, Upper Saddle River, NJ, 1986).
[2] K. Y. Hashimoto, *Surface Acoustic Wave Devices in Telecommunications* (Spring, Berlin, 2000).
[3] D. Morgan, *Surface Acoustic Wave Filters* (Academic Press, Boston, 2007).
[4] S. Shiokawa, Y. Matsui, and T. Moriizumi, Experimental study on liquid streaming by SAW, Japan. J. Appl. Phys. **28**, 126 (1989).
[5] A. Wixforth, Acoustically driven planar microfluidics, Superlattices Microstruct. **33**, 389 (2003).
[6] S. P. Zhan, J. Lata, C. Chen, J. Mai, F. Guo, Z. Tian, L. Ren, Z. Mao, P. H. Huang, P. Li, S. Yang, and T. J. Huang, Digital acoustofluidics enables contactless and programmable liquid handling, Nat. Commun. **9**, 2928 (2018).
[7] W. T. Coakley, D. W. Bardsley, M. A. Grundy, F. Zamani, and D. J. Clarke, Cell manipulation in ultrasonic standing wave fields, J. Chem. Technol. Biotechnol. **44**, 43 (1989).
[8] A. Zemel, F. Rehfeldt, A. E. X. Brown, D. E. Discher, and S. A. Safran, Optimal matrix rigidity for stress-fibre polarization in stem cells, Nat. Phys. **6**, 468 (2010).
[9] M. Stamp, A. Jötten, P. Kudella, D. Breyer, F. Strobl, T. Geislinger, A. Wixforth, and C. Westerhausen, Exploring the limits of cell adhesion under shear stress within physiological conditions and beyond on a chip, Diagnostics **6**, 38 (2016).
[10] H. Wohltjen, Mechanism of operation and design considerations for surface acoustic wave device vapour sensors, Sens. Actuators **5**, 307 (1984).
[11] K. Laenge, B. E. Rapp, and M. Rapp, Surface acoustic wave biosensors: A review, Anal. Bioanal. Chem. **391**, 1509 (2008).
[12] M. Ayaz, M. Ammad-uddin, I. Baig, and E. M. Aggoune, Wireless sensor's civil applications, prototypes, and future integration possibilities: A review, IEEE Sens. J. **18**, 4 (2018).
[13] M. J. A. Schuetz, E. M. Kessler, G. Giedke, L. M. K. Vandersypen, M. D. Lukin, and J. I. Cirac, Universal quantum transducers based on surface acoustic waves, Phys. Rev. X **3**, 031031 (2015).
[14] R. Manenti, A. F. Kockum, A. Patterson, T. Behrle, J. Rahamim, G. Tancredi, F. Nori, and P. J. Leek, Circuit quantum acoustodynamics with surface acoustic waves, Nat. Commun. **8**, 975 (2017).
[15] A. Noguchi, R. Yamazaki, Y. Tabuchi, and Y. Nakamura, Qubit-assisted transduction for a detection of surface acoustic waves near the quantum limit, Phys. Rev. Lett. **119**, 180505 (2017).
[16] C. T. Hann, C.-L. Zou, Y. Zhang, Y. Chu, R. J. Schoelkopf, S. M. Girvin, and L. Jiang, Hardware-efficient quantum random access memory with hybrid quantum acoustic systems, Phys. Rev. Lett. **123**, 250501 (2017).
[17] Y. W. Chu, P. Kharel, W. H. Renninger, L. D. Burkhart, L. Frunzio, P. T. Rakich, and R. J. Schoelkopf, Quantum acoustics with superconducting qubits, Science **358**, 199 (2017).
[18] M. K. Ekström, T. Aref, J. Runeson, J. Björck, I. Boström, and P. Delsing, Surface acoustic wave unidirectional transducers for quantum applications, Appl. Phys. Lett. **110**, 073105 (2017).
[19] G. Andersson, S. W. Jolin, M. Scigliuzzo, R. Borgani, M. O. Tholén, J. C. R. Hernández, V. Shumeiko, D. B. Haviland, and P. Delsing, Squeezing and multimode entanglement of surface acoustic wave phonons, PRX Quantum **3**, 010312 (2022).
[20] M. V. Gustafsson, T. Aref, A. F. Kockum, M. K. Ekström, G. Johansson, and P. Delsing, Propagating phonons coupled to an artificial atom, Science **346**, 207 (2014).
[21] A. N. Bolgar, J. I. Zotova, D. D. Kirichenko, I. S. Besedin, A. V. Semenov, R. S. Shaikhaidarov, and O. V. Astafiev,

Quantum regime of a two-dimensional phonon cavity, Phys. Rev. Lett. **120**, 223603 (2018).

[22] G.-H. Zeng, Y. Zhang, A. N. Bolgar, D. He, B. Li, X.-H. Ruan, L. Zhou, L. M. Kuang, O. V. Astafiev, Y.-X. Liu, and Z. H. Peng, Quantum versus classical regime in circuit quantum acoustodynamics, New J. Phys. **23**, 123001 (2021).

[23] L. Tian and P. Zoller, Coupled ion-nanomechanical systems, Phys. Rev. Lett. **93**, 266403 (2004).

[24] K. R. Brown, C. Ospelkaus, Y. Colombe, A. C. Wilson, D. Leibfried, and D. J. Wineland, Coupled quantized mechanical oscillators, Nature **471**, 196 (2011).

[25] N. Punpongjareorn, X. He, Z. Tang, A. M. Guloy, and D. S. Yang, Ultrafast switching of valence and generation of coherent acoustic phonons in semiconducting rare-earth monosulfides, Appl. Phys. Lett. **111**, 081903 (2022).

[26] M. Benetti, D. Cannata, F. D. Pictrantonio, and E. Verona, Growth of AlN piezoelectric film on diamond for high-frequency surface acoustic wave devices, IEEE Trans. Ultrason. Ferroelectr. Freq. Control **52**, 1806 (2005).

[27] D. A. Golter, T. Oo, M. Amezcua, K. A. Stewart, and H. Wang, Optomechanical quantum control of a nitrogen-vacancy center in diamond, Phys. Rev. Lett. **116**, 143602 (2016).

[28] A. Jung, S. Margueron, A. Bartasyte, and S. Salahuddin, On the coupling between magnetoelastic waves and nitrogen vacancy centers in diamond, Appl. Phys. Lett. **124**, 062406 (2024).

[29] T. Fujisawa, T. H. Oosterkamp, W. G. van der Wiel, B. W. Broer, R. Aguado, S. Tarucha, and L. P. Kouwenhoven, Spontaneous emission spectrum in double quantum dot devices, Science **282**, 932 (1998).

[30] M. Metcalfe, S. M. Carr, A. Muller, G. S. Solomon, and J. Lawall, Resolved sideband emission of InAs/GaAs quantum dots strained by surface acoustic waves, Phys. Rev. Lett. **105**, 037401 (2010).

[31] R. A. DeCrescent, Z. Wang, P. Imany, R. C. Boutelle, C. A. McDonald, T. Autry, J. D. Teufel, S. W. Nam, R. P. Mirin, and K. L. Silverman, Large single-phonon optomechanical coupling between quantum dots and tightly confined surface acoustic waves in the quantum regime, Phys. Rev. Appl. **18**, 034067 (2022).

[32] J. Q. You and F. Nori, Superconducting circuits and quantum information, Phys. Today **58**, 42 (2005).

[33] J. Clarke and F. K. Wilhelm, Superconducting quantum bits, Nature **453**, 1031 (2008).

[34] Z.-L. Xiang, S. Ashhab, J. Q. You, and F. Nori, Hybrid quantum circuits: Superconducting circuits interacting with other quantum systems, Rev. Mod. Phys. **85**, 623 (2013).

[35] X. Gu, A. F. Kockum, A. Miranowicz, Y.-X. Liu, and F. Nori, Microwave photonics with superconducting quantum circuits, Phys. Rep. **718-719**, 1 (2017).

[36] M. Kjaergaard, M. E. Schwartz, J. Braumüller, P. Krantz, J. I. J. Wang, S. Gustavsson, and W. D. Oliver, Superconducting qubits: Current state of play, Annu. Rev. Condens. Matter Phys. **11**, 369 (2020).

[37] A. Bienfait, K. J. Satzinger, Y. P. Zhong, H.-S. Chang, M.-H. Chou, C. R. Conner, É. Dumur, J. Grebel, G. A. Peairs, R. G. Povey, and A. N. Cleland, Phonon-mediated quantum state transfer and remote qubit entanglement, Science **364**, 368 (2019).

[38] S. D. Patel, K. Parto, M. Choquer, N. Lewis, S. Umezawa, L. Hellman, D. Polishchuk, and G. Moody, Surface acoustic wave cavity optomechanics with atomically thin h-BN and WSe_2 single-photon emitters, PRX Quantum **5**, 010330 (2024).

[39] A. Khurana, P. Jiang, and K. C. Balram, Piezo-optomechanical signal transduction using Lamb-wave supermodes in a suspended gallium arsenide photonic-integrated-circuit platform, Phys. Rev. Appl. **18**, 054030 (2022).

[40] D. Hatanaka, M. Asano, H. Okamoto, Y. Kunihashi, H. Sanada, and H. Yamaguchi, On-chip coherent transduction between magnons and acoustic phonons in cavity magnomechanics, Phys. Rev. Appl. **17**, 034024 (2022).

[41] M. K. Ekström, T. Aref, A. Ask, G. Andersson, B. Suri, H. Sanada, G. Johansson, and P. Delsing, Towards phonon routing: Controlling propagating acoustic waves in the quantum regime, New J. Phys. **21**, 123013 (2019).

[42] W. Wang, M. Shen, C.-L. Zou, W. Fu, Z. Shen, and H. X. Tang, High-acoustic-index-contrast phononic circuits: Numerical modeling, J. Appl. Phys. **128**, 184503 (2020).

[43] D. D. Bühler, M. Weiß, A. Crespo-Poveda, E. D. S. Nysten, J. J. Finley, K. Müller, P. V. Santos, M. M. de Lima, and H. J. Krenner, On-chip generation and dynamic piezo-optomechanical rotation of single photons, Nat. Commun. **13**, 6998 (2022).

[44] J. Tang, Y. Wu, Z. Wang, H. Sun, L. Tang, H. Zhang, T. Li, Y. Lu, M. Xiao, and K. Xia, Vacuum-induced surface-acoustic-wave phonon blockade, Phys. Rev. A **101**, 053802 (2020).

[45] T.-S. Yin, G.-R. Jin, and A. X. Chen, Enhanced phonon antibunching in a circuit quantum acoustodynamical system containing two surface acoustic wave resonators, Micromachines **13**, 591 (2022).

[46] W. Z. Xie, Q. Guo, and Z. L. Duan, Phonon blockade in an acoustic cavity coupled to a three-level artificial atom, Phys. Rev. B **106**, 115435 (2022).

[47] A. F. Kockum, P. Delsing, and G. Johansson, Designing frequency-dependent relaxation rates and Lamb shifts for a giant artificial atom, Phys. Rev. A **90**, 013837 (2014).

[48] G. Andersson, B. Suri, L. Guo, T. Aref, and P. Delsing, Non-exponential decay of a giant artificial atom, Nat. Phys. **15**, 1123 (2019).

[49] X. Y. Li, W. Zhao, and Z. H. Wang, Controlling photons by phonons via giant atom in a waveguide QED setup, Opt. Lett. **48**, 3595 (2023).

[50] M. Weiler, L. Dreher, C. Heeg, H. Huebl, R. Gross, M. S. Brandt, and S. T. B. Goennenwein, Elastically driven ferromagnetic resonance in nickel thin films, Phys. Rev. Lett. **106**, 117601 (2011).

[51] R. Sasaki, Y. Nii, Y. Iguchi, and Y. Onose, Nonreciprocal propagation of surface acoustic wave in $Ni/LiNbO_3$, Phys. Rev. B **95**, 020407(R) (2017).

[52] R. Sasaki, Y. Nii, and Y. Onose, Magnetization control by angular momentum transfer from surface acoustic wave to ferromagnetic spin moments, Nat. Commun. **12**, 2599 (2021).

[53] Y. Li, C. Zhao, W. Zhang, A. Hoffmann, and V. Novosad, Advances in coherent coupling between magnons and acoustic phonons, APL Mater. **9**, 060902 (2021).
[54] T. Kikkawa, K. Shen, B. Flebus, R. A. Duine, K. I. Uchida, Z. Y. Qiu, G. E. W. Bauer, and E. Saitoh, Magnon polarons in the spin Seebeck effect, Phys. Rev. Lett. **117**, 207203 (2016).
[55] N. K. P. Babu, A. Trzaskowska, P. Graczyk, G. Centała, S. Mieszczak, H. Głowiński, M. Zdunek, S. Mielcarek, and J. W. Kłos, The interaction between surface acoustic waves and spin waves: The role of anisotropy and spatial profiles of the modes, Nano Lett. **21**, 946 (2021).
[56] Y. Y. Hwang, J. Puebla, K. Kondou, C. Gonzalez-Ballestero, H. Isshiki, C. S. Muñoz, L. Y. Liao, F. Chen, W. Luo, S. Maekawa, and Y. Otani, Strongly coupled spin waves and surface acoustic waves at room temperature, Phys. Rev. Lett. **132**, 056704 (2024).
[57] IEEE Standards Committee, IEEE Standard on magnetostrictive materials: Piezomagnetic nomenclature, IEEE Ultrasonics, Ferroelectrics and Frequency Control Society, Standard 319 (1973).
[58] G. Engdahl, *Handbook of Giant Magnetostrictive Materials* (Academic Press, San Diego, 1999).
[59] J. P. Nowacki, *Static and Dynamic Coupled Fields in Bodies with Piezoeffects or Polarization Gradient* (Springer, Berlin, 2006).
[60] M. E. Peskin and D. V. Schroeder, *An Introduction to Quantum Field Theory* (Addison-Wesley, MA, 1995).
[61] W. Greiner and J. Reinhardt, *Field Quantization* (Springer-Verlag, Berlin, 1996).
[62] See Supplemental Material at http://link.aps.org/supplemental/10.1103/PhysRevApplied.23.034013 for detailed derivations of acoustic wave equations and boundary conditions, solutions of mechanical displacement and magnetic potential, canonical coordinates and canonical momenta, zero-point fluctuation, Hamiltonian of the magnetic quantum systems (i.e., fluxonium qubit, transmon qubit, ferromagnetic magnons, and defect centers) coupling with a quantized single-mode SAW in a piezomagnetic waveguide, and evolutions of population and entanglement. The Supplemental Material also contains Refs. [3,13,52,53,58,60,61,64–67,73,83–90,104–106,126,132,139,140,167–170].
[63] D. Royer and E. Dieulesaint, *Elastic Waves in Solids I* (Springer, Berlin, 2000).
[64] J. D. Jackson, *Classical Electrodynamics* (Wiley, New York, 1999).
[65] A. E. Giannakopoulos and A. Z. Parmaklis, The contact problem of a circular rigid punch on piezomagnetic materials, Int. J. Solids Struct. **44**, 4593 (2007).
[66] L. Rayleigh, On waves propagated along the plane surface of an elastic solid, Proc. Lond. Math. Soc. **17**, 4 (1885).
[67] D. L. T. Bell and R. C. M. Li, Surface-acoustic-wave resonators, Proc. IEEE **64**, 711 (1976).
[68] V. Kottamasu, Magnetostrictive elastic wave-type linear motion with terfenol-D, Proc. SPIE **3044**, 363 (1997).
[69] S. Chakrabarti and M. J. Dapino, Hydraulically amplified terfenol-D actuator for adaptive powertrain mounts, J. Vib. Acoust. **133**, 061015 (2011).
[70] A. G. Olabi and A. Grunwald, Design and application of magnetostrictive materials, Mater. Design. **29**, 469 (2008).
[71] A. A. Zakharenko, A study of SH-SAW propagation in cubic piezomagnetics for utilization in smart materials, Wave Random Complex **22**, 488 (2012).
[72] P. B. Li and F. Nori, Hybrid quantum system with nitrogen-vacancy centers in diamond coupled to surface-phonon polaritons in piezomagnetic superlattices, Phys. Rev. Appl. **10**, 024011 (2018).
[73] S. M. Dutra, *Cavity Quantum Electrodynamics: The Strange Theory of Light in a Box* (Wiley, New York, 2005).
[74] M. M. de Lima Jr and P. V. Santos, Modulation of photonic structures by surface acoustic waves, Rep. Prog. Phys. **68**, 1639 (2005).
[75] W. Fu, Z. Shen, Y. T. Xu, C.-L. Zou, R. S. Cheng, X. Han, and H. X. Tang, Phononic integrated circuitry and spin-orbit interaction of phonons, Nat. Commun. **10**, 2743 (2019).
[76] L. B. Shao, D. Zhu, M. Colangelo, D. Lee, N. Sinclair, Y. W. Hu, P. T. Rakich, K. J. Li, K. K. Beggren, and M. Lončar, Electrical control of surface acoustic waves, Nat. Electron. **5**, 348 (2022).
[77] Y. L. Liu, Q. C. Liu, H. Y. Sun, M. Chen, S. P. Wang, and T. F. Li, Coherent memory for microwave photons based on long-lived mechanical excitations, Npj Quantum Inf. **9**, 80 (2023).
[78] C. L. Wang *et al.*, Towards practical quantum computers: Transmon qubit with a lifetime approaching 0.5 milliseconds, Npj Quantum Inf. **8**, 3 (2022).
[79] R. C. Jaklevic, J. Lambe, A. H. Silver, and J. E. Mercereau, Quantum interference effects in Josephson tunneling, Phys. Rev. Lett. **12**, 159 (1964).
[80] J. Clarke, W. M. Goubau, and M. B. Ketchen, Tunnel junction dc SQUID: Fabrication, operation, and performance, J. Low Temp. Phys. **25**, 99 (1976).
[81] K. K. Likharev, *Dynamics of Josephson Junctions and Circuits* (Gordon and Breach Science Publishers, New York, 1986).
[82] Y. Makhlin, G. Scöhn, and A. Shnirman, Josephson-junction qubits with controlled couplings, Nature **398**, 305 (1999).
[83] V. E. Manucharyan, J. Koch, L. I. Glazman, and M. H. Devoret, Fluxonium: Single Cooper-pair circuit free of charge offsets, Science **326**, 113 (2009).
[84] G. Y. Zhu, D. G. Ferguson, V. E. Manucharyan, and J. Koch, Circuit QED with fluxonium qubits: Theory of the dispersive regime, Phys. Rev. B **87**, 024510 (2013).
[85] N. Earnest, S. Chakram, Y. Lu, N. Irons, R. K. Naik, N. Leung, L. Ocola, D. A. Czaplewski, B. Baker, J. Lawrence, J. Koch, and D. I. Schuster, Realization of a Λ system with metastable states of a capacitively shunted fluxonium, Phys. Rev. Lett. **120**, 150504 (2018).
[86] L. B. Nguyen, G. Koolstra, Y. Kim, A. Morvan, T. Chistolini, S. Singh, K. N. Nesterov, C. Jünger, L. Chen, Z. Pedramrazi, B. K. Mitchell, J. M. Kreikebaum, S. Puri, D. I. Santiago, and I. Siddiqi, Blueprint for a high-performance fluxonium quantum processor, PRX Quantum **3**, 037001 (2022).

[87] J. Koch, T. M. Yu, J. Gambetta, A. A. Houck, D. I. Schuster, J. Majer, A. Blais, and M. H. Devoret, Charge-insensitive qubit design derived from the Cooper pair box, Phys. Rev. A **76**, 042319 (2007).

[88] A. A. Houck, J. A. Schreier, B. R. Johnson, J. M. Chow, J. Koch, J. M. Gambetta, D. I. Schuster, L. Frunzio, M. H. Devoret, S. M. Girvin, and R. J. Schoelkopf, Controlling the spontaneous emission of a superconducting transmon qubit, Phys. Rev. Lett. **101**, 080502 (2008).

[89] Y. Kubo, C. Grezes, A. Dewes, T. Umeda, J. Isoya, H. Sumiya, N. Morishita, H. Abe, S. Onoda, T. Ohshima, V. Jacques, A. Dréau, J. F. Roch, I. Diniz, A. Auffeves, D. Vion, D. Esteve, and P. Bertet, Hybrid quantum circuit with a superconducting qubit coupled to a spin ensemble, Phys. Rev. Lett. **107**, 220501 (2011).

[90] M. J. Peterer, S. J. Bader, X. Y. Jin, F. Yan, A. Kamal, T. J. Gudmundsen, P. J. Leek, T. P. Orlando, W. D. Oliver, and S. Gustavsson, Coherence and decay of higher energy levels of a superconducting transmon qubit, Phys. Rev. Lett. **114**, 010501 (2015).

[91] S. L. Chao, Z. Yang, C. S. Zhao, R. Peng, and L. Zhou, Force sensing in a dual-mode optomechanical system with linear-quadratic coupling and modulated photon hopping, Opt. Lett. **46**, 3075 (2021).

[92] Y. H. Yang, X. B. Xu, J. Q. Wang, M. Zhang, M. Li, Z. X. Zhu, Z. B. Wang, C. H. Dong, W. Fang, H. K. Yu, G. C. Guo, and C. L. Zou, Nonlinear optical radiation of a lithium niobate microcavity, Phys. Rev. Appl. **19**, 034087 (2023).

[93] S. Puri and A. Blais, High-fidelity resonator-induced phase gate with single-mode squeezing, Phys. Rev. Lett. **116**, 180501 (2016).

[94] Y. F. Ye, K. D. Peng, M. Naghiloo, G. Cunningham, and K. P. O'Brien, Engineering purely nonlinear coupling between superconducting qubits using a quarton, Phys. Rev. Lett. **127**, 050502 (2021).

[95] T. Tanamoto, Y.-X. Liu, S. Fujita, X. D. Hu, and F. Nori, Producing cluster states in charge qubits and flux qubits, Phys. Rev. Lett. **97**, 230501 (2006).

[96] X. Ma, J. J. Viennot, S. Kotler, J. D. Teufel, and K. W. Lehnert, Non-classical energy squeezing of a macroscopic mechanical oscillator, Nat. Phys. **17**, 322 (2021).

[97] A. Nunnenkamp, K. Børkje, J. G. E. Harris, and S. M. Girvin, Cooling and squeezing via quadratic optomechanical coupling, Phys. Rev. A **82**, 021806(R) (2010).

[98] N. P. Bullier, A. Pontin, and P. F. Barker, Quadratic optomechanical cooling of a cavity-levitated nanosphere, Phys. Rev. Res. **3**, L032022 (2021).

[99] N. E. Frattini, V. V. Sivak, A. Lingenfelter, S. Shankar, and M. H. Devoret, Optimizing the nonlinearity and dissipation of a SNAIL parametric amplifier for dynamic range, Phys. Rev. Appl. **10**, 054020 (2018).

[100] R. Yanagimoto, R. Nehra, R. Hamerly, E. Ng, A. Marandi, and H. Mabuchi, Quantum nondemolition measurements with optical parametric amplifiers for ultrafast universal quantum information processing, PRX Quantum **4**, 010333 (2023).

[101] M. Bild, M. Fadel, Y. Yang, U. V. Lüpke, P. Martin, A. Bruno, and Y. W. Chu, Schrödinger cat states of a 16-microgram mechanical oscillator, Science **380**, 274 (2023).

[102] H. Qiao, É. Dumur, G. Andersson, H. Yan, M.-H. Chou, J. Grebel, C. R. Conner, Y. J. Joshi, J. M. Miller, R. G. Povey, X. Wu, and A. N. Cleland, Splitting phonons: Building a platform for linear mechanical quantum computing, Science **380**, 1030 (2023).

[103] Ö. O. Soykal and M. E. Flatté, Strong field interactions between a nanomagnet and a photonic cavity, Phys. Rev. Lett. **104**, 077202 (2010).

[104] B. Z. Rameshti, S. V. Kusminski, J. A. Haigh, K. Usami, D. Lachance-Quirion, Y. Nakamura, C. M. Hu, H. X. Tang, G. E. W. Bauer, and Y. M. Blanter, Cavity magnonics, Phys. Rep. **979**, 1 (2022).

[105] L. Dreher, M. Weiler, M. Pernpeintner, H. Huebl, R. Gross, M. S. Brandt, and S. T. B. Goennenwein, Surface acoustic wave driven ferromagnetic resonance in nickel thin films: Theory and experiment, Phys. Rev. B **86**, 134415 (2012).

[106] C. Kittel, On the theory of ferromagnetic resonance absorption, Phys. Rev. **73**, 155 (1948).

[107] Y. Tabuchi, S. Ishino, T. Ishikawa, R. Yamazaki, K. Usami, and Y. Nakamura, Hybridizing ferromagnetic magnons and microwave photons in the quantum limit, Phys. Rev. Lett. **113**, 083603 (2014).

[108] X. Zhang, C.-L. Zou, L. Jiang, and H. X. Tang, Strongly coupled magnons and cavity microwave photons, Phys. Rev. Lett. **113**, 156401 (2014).

[109] D. Zhang, X. Q. Luo, Y. P. Wang, T. F. Li, and J. Q. You, Observation of the exceptional point in cavity magnon-polaritons, Nat. Commun. **8**, 1368 (2017).

[110] G. Schmidt, C. Hauser, P. Trempler, M. Paleschke, and E. T. Papaioannou, Ultra thin films of yttrium iron garnet with very low damping: A review, Phys. Status Solidi B **257**, 1900644 (2020).

[111] S. Yuan, C. Liu, J. Chen, S. Liu, J. Lan, H. Yu, J. Wu, F. Yan, M. H. Yung, J. Xiao, L. Jiang, and D. P. Yu, Spin-wave-based tunable coupler between superconducting flux qubits, Phys. Rev. A **107**, 012434 (2023).

[112] Z. Shen, G. T. Xu, M. Zhang, Y. L. Zhang, Y. Wang, C. Z. Chai, C.-L. Zou, G. C. Guo, and C. H. Dong, Coherent coupling between phonons, magnons, and photons, Phys. Rev. Lett. **129**, 243601 (2022).

[113] A. G. Krause, M. Winger, T. D. Blasius, Q. Lin, and O. Painter, A high-resolution microchip optomechanical accelerometer, Nat. Photonics **6**, 768 (2012).

[114] C. A. Potts, V. A. S. V. Bittencourt, S. V. Kusminskiy, and J. P. Davis, Magnon-phonon quantum correlation thermometry, Phys. Rev. Appl. **13**, 064001 (2020).

[115] V. Fiore, Y. Yang, M. C. Kuzyk, R. Barbour, L. Tian, and H. L. Wang, Storing optical information as a mechanical excitation in a silica optomechanical resonator, Phys. Rev. Lett. **107**, 133601 (2011).

[116] B. Sarma, T. Busch, and J. Twamley, Cavity magnomechanical storage and retrieval of quantum states, New J. Phys. **23**, 043041 (2021).

[117] P. Grünberg, R. Schreiber, Y. Pang, M. B. Brodsky, and H. Sowers, Layered magnetic structures: Evidence for antiferromagnetic coupling of Fe layers across Cr interlayers, Phys. Rev. Lett. **57**, 2442 (1986).

[118] J. A. C. Bland and B. Heinrich, *Ultrathin Magnetic Structure III* (Springer, Berlin, 2005).
[119] Y. Li, W. Cao, V. P. Amin, Z. Z. Zhang, J. Gibbons, J. Sklenar, J. Pearson, P. M. Haney, M. D. Stiles, W. E. Bailey, V. Novosad, A. Hoffmann, and W. Zhang, Coherent spin pumping in a strongly coupled magnon-magnon hybrid system, Phys. Rev. Lett. **124**, 117202 (2020).
[120] R. A. Gallardo, T. Schneider, A. K. Chaurasiya, A. Oelschlägel, S. S. P. K. Arekapudi, A. Roldán-Molina, R. Hübner, K. Lenz, A. Barman, J. Fassbender, J. Lindner, O. Hellwig, and P. Landeros, Reconfigurable spin-wave nonreciprocity induced by dipolar interaction in a coupled ferromagnetic bilayer, Phys. Rev. Appl. **12**, 034012 (2019).
[121] M. Ishibashi, Y. Shiota, T. Li, S. Funada, T. Moriyama, and T. Ono, Switchable giant nonreciprocal frequency shift of propagating spin waves in synthetic antiferromagnets, Sci. Adv. **6**, eaaz6931 (2020).
[122] M. Asano, H. Matsumoto, M. Hayashi, and D. Hatanaka, Cavity magnomechanical coupling with coupled magnon modes in a synthetic antiferromagnet, Phys. Rev. B **108**, 064415 (2023).
[123] H. Matsumoto, I. Yasuda, M. Asano, Y. Todaka, T. Kawada, M. Kawaguchi, D. Hatanaka, and M. Hayashi, Magnon-phonon coupling of synthetic antiferromagnets in a surface acoustic wave cavity resonator, Nano Lett. **24**, 5683 (2024).
[124] S. Parkin, X. Jiang, C. Kaiser, A. Panchula, K. Roche, and M. Samant, Magnetically engineered spintronic sensors and memory, Proc. IEEE **91**, 661 (2003).
[125] L. Liu, C. H. Zhou, X. Y. Shu, C. J. Li, T. Y. Zhao, W. N. Lin, J. Y. Deng, Q. D. Xie, S. H. Chen, J. Zhou, R. Guo, H. Wang, J. H. Yu, S. Shi, P. Yang, S. Pennycook, A. Manchon, and J. S. Chen, Symmetry-dependent field-free switching of perpendicular magnetization, Nat. Nanotechnol. **16**, 277 (2021).
[126] L. Rondin, J. P. Tetienne, T. Hingant, J. F. Roch, P. Maletinsky, and V. Jacques, Magnetometry with nitrogen-vacancy defects in diamond, Rep. Prog. Phys. **77**, 056503 (2014).
[127] A. Gruber, A. Dräbenstedt, C. Tietz, L. Fleury, J. Wrachtrup, and C. von Borczyskowski, Scanning confocal optical microscopy and magnetic resonance on single defect centers, Science **256**, 2012 (1997).
[128] P. Tamarat, T. Gaebel, J. R. Rabeau, M. Khan, A. D. Greentree, H. Wilson, L. C. L. Hollenberg, S. Prawer, P. Hemmer, F. Jelezko, and J. Wrachtrup, Stark shift control of single optical centers in diamond, Phys. Rev. Lett. **97**, 083002 (2006).
[129] V. Jacques, P. Neumann, J. Beck, M. Markham, D. Twitchen, J. Meijer, F. Kaiser, G. Balasubramanian, F. Jelezko, and J. Wrachtrup, Dynamic polarization of single nuclear spins by optical pumping of nitrogen-vacancy color centers in diamond at room temperature, Phys. Rev. Lett. **102**, 057403 (2009).
[130] G. D. Fuchs, G. Burkard, P. V. Klimov, and D. D. Awschalom, A quantum memory intrinsic to single nitrogen-vacancy centres in diamond, Nat. Phys. **7**, 789 (2011).
[131] J. Cai, F. Jelezko, and M. B. Plenio, Hybrid sensors based on colour centres in diamond and piezoactive layers, Nat. Commun. **5**, 4065 (2014).
[132] P. Udvarhelyi, V. O. Shkolnikov, A. Gali, G. Burkard, and A. Pályi, Spin-strain interaction in nitrogen-vacancy centers in diamond, Phys. Rev. B **98**, 075201 (2018).
[133] S. D. Bennett, N. Y. Yao, J. Otterbach, P. Zoller, P. Rabl, and M. D. Lukin, Phonon-induced spin-spin interactions in diamond nanostructures: Application to spin squeezing, Phys. Rev. Lett. **110**, 156402 (2013).
[134] M. J. Zhu, J. H. Li, M. Toda, and T. Ono, Microfabrication of a scanning probe with NV centers in a selectively grown diamond thin film through a xenon difluoride etching process, J. Micromech. Microeng. **27**, 125007 (2017).
[135] P. K. Shandilya, D. P. Lake, M. J. Mitchell, D. D. Sukachev, and P. E. Barclay, Optomechanical interface between telecom photons and spin quantum memory, Nat. Phys. **17**, 1420 (2021).
[136] H. Raniwala, S. Krastanov, L. Hackett, M. Eichenfield, D. R. Englund, and M. E. Trusheim, Piezoelectric nanocavity interface for strong coupling between a superconducting circuit, phonon, and spin, Phys. Rev. Appl. **19**, 064051 (2023).
[137] K. Ohashi, T. Rosskopf, H. Watanabe, M. Loretz, Y. Tao, R. Hauert, S. Tomizawa, T. Ishikawa, J. Ishi-Hayase, S. Shikata, C. L. Degen, and K. M. Itoh, Negatively charged nitrogen-vacancy centers in a 5 nm thin ^{12}C diamond film, Nano Lett. **13**, 4733 (2013).
[138] R. Amsüss, Ch. Koller, T. Nöbauer, S. Putz, S. Rotter, K. Sandner, S. Schneider, M. Schramböck, G. Steinhauser, H. Ritsch, J. Schmiedmayer, and J. Majer, Cavity QED with magnetically coupled collective spin states, Phys. Rev. Lett. **107**, 060502 (2011).
[139] W. K. Wootters, Entanglement of formation of an arbitrary state of two qubits, Phys. Rev. Lett. **80**, 2245 (1998).
[140] G. S. Agarwal, *Quantum Optics* (Cambridge University Press, UK, 2013).
[141] U. Dorner and P. Zoller, Laser-driven atoms in half-cavities, Phys. Rev. A **66**, 023816 (2002).
[142] I.-C. Hoi, A. F. Kockum, L. Tornberg, A. Pourkabirian, G. Johansson, P. Delsing, and C. M. Wilson, Probing the quantum vacuum with an artificial atom in front of a mirror, Nat. Phys. **10**, 1038 (2015).
[143] F. Dubin, D. Rotter, M. Mukherjee, C. Russo, J. Eschner, and R. Blatt, Photon correlation versus interference of single-atom fluorescence in a half-cavity, Phys. Rev. Lett. **98**, 183003 (2007).
[144] H. Andreas and G.-O. Ricardo, Higher-order chemical sensing, Chem. Rev. **108**, 563 (2008).
[145] K. Bodenhöfer, A. Hierlemann, J. Seemann, G. Gauglitz, B. Koppenhoefer, and W. Göpel, Chiral discrimination using piezoelectric and optical gas sensors, Nature **387**, 577 (1997).
[146] G. Calajó, M. J. A. Schuetz, H. Pichler, M. D. Lukin, P. Schneeweiss, J. Volz, and P. Rabl, Quantum acousto-optic control of light-matter interactions in nanophotonic networks, Phys. Rev. A **99**, 053852 (2019).
[147] A. C. Poveda, D. D. Bühler, A. C. Sáez, P. V. Santos, and M. M. de Lima Jr, Semiconductor optical waveguide

devices modulated by surface acoustic waves, J. Phys. D: Appl. Phys. **52**, 253001 (2019).

[148] G. P. Carman and M. Mitrovic, Nonlinear constitutive relations for magnetostrictive materials with applications to 1-D problems, J. Intel. Mat. Syst. Str. **6**, 673 (1995).

[149] M. Jaime, A. Saul, M. Salamon, V. S. Zapf, N. Harrison, T. Durakiewicz, J. C. Lashley, D. A. Andersson, C. R. Stanek, J. L. Smith, and K. Gofryk, Piezomagnetism and magnetoelastic memory in uranium dioxide, Nat. Commun. **8**, 99 (2017).

[150] C. H. Lin and Y. Z. Lin, Analysis of nonlinear piezomagnetism for magnetostrictive terfenol-D composites, J. Magn. Magn. Mater. **540**, 168490 (2021).

[151] Q. K. Meng, J. T. Dong, P. Nie, L. C. Xu, J. H. Wang, S. Jiang, H. K. Zuo, J. Zhang, X. K. Li, Z. W. Zhu, L. Balents, and K. Behnia, Magnetostriction, piezomagnetism and domain nucleation in a Kagome antiferromagnet, Nat. Commun. **15**, 6921 (2024).

[152] R. Inaba and N. Mikosgiba, Parametric amplification of surface acoustic wave of ZnO-Ga-doped yttrium iron garnet, Appl. Phys. Lett. **100**, 192410 (1982).

[153] B. D. Zaitsev, A. V. Ermolenko, and V. A. Fedorenko, Magnetoacoustic SAW interaction in YIG films, IEEE Trans. Ultrason. Ferroelectr. Freq. Control **45**, 356 (1998).

[154] A. V. Chumak, P. Dhagat, A. Jander, A. A. Serga, and B. Hillebrands, Reverse Doppler effect of magnons with negative group velocity scattered from a moving Bragg grating, Phys. Rev. B **81**, 140404(R) (2010).

[155] R. G. Kryshtal and A. V. Medved, Nonlinear spin waves in dynamic magnonic crystals created by surface acoustic waves in yttrium iron garnet films, J. Phys. D: Appl. Phys. **50**, 495004 (2017).

[156] A. V. Azovtsev and N. A. Pertsev, Dynamical spin phenomena generated by longitudinal elastic waves traversing $CoFe_2O_4$ films and heterostructures, Phys. Rev. B **100**, 224405 (2019).

[157] S. H. Zhuang and J. M. Hu, Acoustic attenuation in magnetic insulator films: Effects of magnon polaron formation, J. Phys. D: Appl. Phys. **56**, 054004 (2023).

[158] S. H. Zhuang, X. F. Zhang, Y. J. Zhu, N. X. Sun, C. B. Eom, P. G. Evans, and J. M. Hu, Hybrid magnon-phonon cavity for large-amplitude terahertz spin-wave excitation, Phys. Rev. Appl. **21**, 044009 (2024).

[159] K. B. Hathaway, A. E. Clark, and J. P. Teter, Magnetomechanical damping in giant magnetostriction alloys, Metall. Mater. Trans. A **26**, 2797 (1995).

[160] C. A. Kerrigan, K. K. Ho, K. P. Mohanchandra, and G. P. Carman, Microscale damping using thin film active materials, Proc. SPIE **6525**, 65250V (2007).

[161] Y. P. Yao, Y. Hou, S. N. Dong, X. H. Huang, Q. X. Yu, and X. G. Li, Influence of magnetic fields on the mechanical loss of terfenol-D/$PbZr_{0.52}Ti_{0.48}O_3$/terfenol-D laminated composites, J. Alloys Compd. **509**, 6920 (2011).

[162] M. S. Fashami, K. Roy, J. Atulasimha, and S. Bandyopadhyay, Magnetization dynamics, Bennett clocking and associated energy dissipation in multiferroic logic, Nanotechnology **22**, 155201 (2011).

[163] O. Kovalenko and T. Pezeril, New concept for magnetization switching by ultrafast acoustic pulses, Phys. Rev. Lett. **110**, 266602 (2013).

[164] D. B. Gopman, J. W. Lau, K. P. Mohanchandra, K. Wetzlar, and G. P. Carman, Determination of the exchange constant of $Tb_{0.3}Dy_{0.7}Fe_2$ by broadband ferromagnetic resonance spectroscopy, Phys. Rev. B **93**, 064425 (2016).

[165] W. H. Louisell, *Quantum Statistical Properties of Radiation* (Wiley, New York, 1973).

[166] C. W. Gardiner and P. Zoller, *Quantum Noise* (Spring, Berlin, 2000).

[167] T. Kobayashi, R. C. Barker, J. L. Bleustein, and A. Yelon, Ferromagnetoelastic resonance in thin films. I. Formal treatment, Phys. Rev. B **7**, 3273 (1973).

[168] T. Holstein and H. Primakoff, Field dependence of the intrinsic domain magnetization of a ferromagnet, Phys. Rev. **58**, 1098 (1940).

[169] A. Klein and E. R. Marshalek, Boson realizations of Lie algebras with applications to nuclear physics, Rev. Mod. Phys. **63**, 375 (1991).

[170] X. F. Zhang, C. L. Zou, L. Jiang, and H. X. Tang, Cavity magnomechanics, Sci. Adv. **2**, e1501286 (2016).